Mathematics Notes

Note 82

31 March 1984

Use of Complex Demodulation in Analyzing Transient Responses

H. T. Davis
Dikewood, Division of
Kaman Sciences Corporation
Albuquerque, New Mexico 87102

ABSTRACT

This report deals with two numerical methods for estimating the natural modes used to characterize the response of a conducting body to an incident electromagnetic pulse (EMP) wave. These are Prony's method and complex demodulation. The two methods are compared for several simulated conditions and complex demodulation is demonstrated on actual pin current realizations. It is concluded that complex demodulation is a very flexible tool for analyzing transient data.

PREFACE

The author wishes to express his gratitude to Captain Tom Marshall and W. Prather of AFWL, June Brenton and Lennart Marin of Dikewood, Division of Kaman Sciences Corporation, and J. P. Castillo and William Kehrer of RDA, for their generous contributions to this report.

CONTENTS

I. INTRODUCTION

1. BACKGROUND

An electromagnetic pulse (EMP) incident on an aircraft system induces currents on the skin, which then couple through points of entry in the surface to induce currents on the wires connected to electronic components inside the aircraft. The currents are of short duration, typically 2 to 5 μs, and are typically sampled at intervals of 1 to 20 ns. For any meaningful analysis, the data have to be converted into physical parameters. The singularity expansion method (SEM) provides a reasonable way to parameterize the system response.

The SEM introduced by Baum (Ref. 1) provides a physically meaningful way to characterize a conducting body's response to EMP. The response of a conducting body to an incident EMP wave is expressed as a sum of complex exponentials using parameters related to the natural modes of the conducting body. This parameterization not only reduces the amount of data required to characterize a sample realization, but also reduces it to terms that are physically useful. Ideally, the parameters can be predicted from models of the aircraft surface. However, the complexity of an aircraft surface makes it difficult to formulate and solve the scattering problem for an exact aircraft model. Therefore, simplified models, which preserve the global features of the aircraft, are used to obtain mathematically tractable solutions. This makes it important to have numerical methods of estimating the natural modes from data.

This report deals with two numerical methods for estimating the natural modes from data. The first, Prony's method, is not new but has been widely used in this and other similar applications. The second method, complex demodulation, is also not new; however, its application to modal analysis is new. The two methods are compared for several simulated conditions, and complex demodulation is demonstrated on actual pin current realizations.

2. PRONY'S METHOD

Consider a metallic object excited by a plane wave field incident at an angle of incidence (ϕ,θ). Using the SEM representation (Refs. 1 and 2), the induced current at a point x on the surface of the aircraft can be written in the form

$$I(x,t) = \sum_{i=1}^{M} c_i(x,\phi,\theta)\, e^{s_i t} + g(x,\phi,\theta,t) \qquad (1)$$

where s_i are the natural complex frequencies or poles of the scatterer, c_i the corresponding residues at s_i, and g(t) the forced response. The arguments x, ϕ, and θ will be suppressed in this paper. The responses due to the systems natural modes can be expressed as

$$y_t = \sum_{i=1}^{M} c_i\, e^{s_i t} \qquad (2)$$

Since this response is a real function of time, the s_i must either be real or occur in complex conjugate pairs. Let y(k) be the natural response sampled at equal time intervals with a total of N points, then

$$y(k) = \sum_{i=1}^{M} c_i\, e^{s_i k\Delta T}$$

$$k = 0,1,2,\ldots,N-1 \qquad (3)$$

where ΔT is the sampling interval. Equation 3 can be rewritten as

$$y(k) = \sum_{i=1}^{M} c_i\, z_i^k$$

$$k = 0,1,2,\ldots,N-1 \qquad (4)$$

with

$$z_i = e^{s_i \Delta t}$$

With this set of equations, the problem is to solve for both the M values of z_i and the M values of c_i. It is assumed that the value of N, the amount of data collected, is at least 2M, the number of parameters to be estimated. The solution to this set of equations is nontrivial, since they are nonlinear in z_i.

Let $z_1, z_2, \ldots, z_M$ be the roots of the algebraic equation

$$z^M = \sum_{i=1}^{M} a_i\, z^{M-i} \qquad (5)$$

In order to determine the coefficients $a_1,\ldots,a_M$, Equations 4 and 5 can be used to show (Ref. 2) that the data $y(k)$ satisfy the difference equation

$$y(j) = \sum_{i=1}^{M} a_i\, y(j-i)$$

$$j = M+1, M+2, \ldots, N \tag{6}$$

It should be pointed out that the notation in Equation 5 differs from that of Reference 2 in which the coefficients $\{a_i\}$ have the opposite sign.

In general, it is possible to use the first M equations to solve for the linear coefficients $a_1,\ldots,a_M$,

$$\begin{bmatrix} y(M+1) \\ \vdots \\ y(2M) \end{bmatrix} = \begin{bmatrix} y(M) & \cdots & y(1) \\ \vdots & & \vdots \\ y(2M-1) & \cdots & y(M+1) \end{bmatrix} \begin{bmatrix} a(1) \\ \vdots \\ a(M) \end{bmatrix} \tag{7}$$

in Equation 6. Then a root solving routine can be used to obtain the roots to Equation 5, $z_1,\ldots,z_M$ where the z_i are representatives of $y(k)$ in Equation 4. With the z_i obtained, the first M values of $y(k)$ can be used with Equation 4 to obtain the residues c_i. Also, the roots s_i in Equation 3 can be obtained from Equation 4, i.e.,

$$s_i = \frac{\ln z_i}{\Delta T} \tag{8}$$

In practice, however, it is not so easy. One serious problem is that the data values are typically noise corrupted. A second problem is that the data values observed are not the natural responses $y(k)$, but rather $I(t)$, which have the force functions $g(k\Delta T)$ added. The obvious solution to both problems is to use all N-M equations in a least-squares solution to estimate $a_1,\ldots,a_M$. That is,

$$\begin{bmatrix} y(M+1) \\ \vdots \\ y(2M) \\ \vdots \\ y(N) \end{bmatrix} = \begin{bmatrix} y(M) & \cdots & y(1) \\ \vdots & & \vdots \\ y(2M-1) & \cdots & y(M+1) \\ \vdots & & \vdots \\ y(N-1) & \cdots & y(N-M) \end{bmatrix} \begin{bmatrix} a(1) \\ \vdots \\ a(M) \end{bmatrix} + \begin{bmatrix} e(M+1) \\ \vdots \\ e(2M) \\ \vdots \\ e(N) \end{bmatrix} \tag{9}$$

where e(k) represents noise and the forced function. Representing Equation 9 in matrix notation,

$$Y = Ha + e \tag{10}$$

then the least-squares estimator of the vector a is the solution to the normal equations

$$H^T H\, a = H^T Y \tag{11}$$

Two difficulties arise in this approach. The first comes from modeling the driven response as noise, since in early time the response has very large magnitude and least squares is highly sensitive to non-homogeneous noise (i.e., when the variance of e(t) is not constant in time). Second, the true regression model is

$$I(k\Delta t) = \sum_{i=1}^{M} a_i\, y(k-i) + e(k) \tag{12}$$

where the regressor variable y(t) is unobserved. This latter problem will be returned to in Section I.4, but in this paper the first problem will be shown to be a very significant problem. In particular, when the signal-to-noise ratio is large, the damped exponential model is not appropriate; and when the damped exponential model finally becomes appropriate, the signal-to-noise ratio has diminished.

3. TIME SERIES MODEL

There is a relationship between the Prony method and a method found in time series literature. A model of the form

$$Y_t = \sum_{i=1}^{M} a_i\, Y_{t-i} + \varepsilon_t \tag{13}$$

where $\{\varepsilon_t\}$ is a white noise process, is referred to as an autoregressive process, since the process is regressed on its own past. The autoregressive model can be viewed as a linear filter, with a linear impluse response function characterized by the $\{a_i\}$ and white noise input.

There is no formal difference between the autoregressive model given in Equation 13 and the linear regression solution to the Prony method in Equation

9 if the residuals are assumed to be uncorrelated homogeneous random variables. There are differences in fact, however, because the problem at hand is one of analyzing a deterministic transient response while the time series literature deals with weakly stationary series. This difference is the problem noted after Equation 12. The estimation methods, however, are similar.

The parameters of an autoregressive process are typically estimated by the Yule-Walker equations,

$$R(k) = \sum_{i=1}^{M} a_i \, R(k - i)$$

$$k = 1,2,... \tag{14}$$

where the R(k) is the autocovariance function

$$R(k) = E[\{Y(t) - E[Y(t)]\}\{Y(t + k) - E[Y(t)\}] \tag{15}$$

Using the first M equations,

$$\begin{bmatrix} R(1) \\ R(2) \\ \cdot \\ \cdot \\ \cdot \\ R(M) \end{bmatrix} = \begin{bmatrix} R(0) & R(1) & \cdots & R(M-1) \\ R(1) & R(0) & & R(M-2) \\ \cdot & \cdot & & \cdot \\ \cdot & \cdot & & \cdot \\ \cdot & \cdot & & \cdot \\ R(M-1) & R(M-2) & \cdots & R(0) \end{bmatrix} \begin{bmatrix} a(1) \\ a(2) \\ \cdot \\ \cdot \\ \cdot \\ a(M) \end{bmatrix} \tag{16}$$

one can easily obtain estimates of the a(k). In practice, however, the covariance function is unknown. In this case, the estimated covariance function

$$r(k) = \frac{1}{N} \sum_{i=1}^{N-k} Y(i) \, Y(i+k) \tag{17}$$

is used. Asymptotically, the Yule-Walker equations (Eq. 16) with the estimated covariance function (Eq. 17), and the normal equations (Eq. 11) are the same. Several algorithms for solving the Yule-Walker equations utilize this fact and solve the equivalent linear regression problem.

A condition for an autoregressive process to be weakly stationary is that the roots of the characteristic equation (Eq. 5) be inside the unit circle.

Further, it is known that as the roots approach the unit circle, the estimates of the parameters of the autoregressive process become severely biased. Also, the Yule-Walker equations themselves become ill-conditioned making the numerical solution difficult. By the relationship in Equation 4 between the roots z_i and the natural frequencies, it follows that

$$z_k = e^{-\alpha_k \Delta T} \; e^{i\omega_k \Delta T} \tag{18}$$

where

$$s_k = -\alpha_k + i\omega_k$$

is the kth natural frequency. As $\alpha_k \Delta T$ becomes small, the magnitude of z_k approaches 1. A small value of α will make a root approach the unit circle, but also a small sampling interval (small ΔT) makes all of the roots approach the unit circle.

An interesting concept from time series literature is that of partial correlation. A rough definition of the kth partial correlation is that it is the correlation between Y_t and Y_{t+k} when the information in the intervening variables, $Y_{t+1},\ldots,Y_{t+k-1}$, has been accounted for. It is used widely in time series to decide when to stop adding terms to the autoregression (i.e., selecting the number of roots). A sufficient condition for the time series to be weakly stationary and the roots of the characteristic equation to be inside the unit circle is that all the partial correlations be less than unity in magnitude (Ref. 3).

4. AUTOREGRESSION PLUS NOISE

The problem of observing the total current and not the natural response (Eq. 12) has received considerable attention in the Prony literature. Since $I(k\Delta T) = y(k) + e(k)$ is observed, it is possible to substitute in Equation 12 and obtain

$$I(k\Delta T) = \sum_{i=1}^{M} a_i \, I[(k - i)\Delta T] + e(k) - \sum_{i=i}^{M} a_i \, e(k - i) \tag{19}$$

Numerous papers exist in the time series literature on estimation of an autoregressive process plus noise (Refs. 4 and 5). A very simple notion is to

note that the colored noise has no effect on the covariance for lags greater than M, that is, the Yule-Walker equations

$$R(k) = \sum_{i=1}^{M} a_i \, R(k - i) \tag{20}$$

still hold for

$$k = M+1, M+2, \ldots$$

By shifting to the next M Yule-Walker equations, the added noise is not a factor. A more stable solution is outlined in Reference 5.

Another solution to this problem, found in the Prony literature, is the iterative premultiply method (Ref. 2). The method simply involves iteratively solving the problem as weighted regression, using the autoregressive structure to compute the covariance of the noise process in Equation 19. While this improves the performance of Prony (Ref. 2), there is still a difficulty because of the transient nature of the driven response. The covariance function used is correct if the e(t) process is white noise. Unfortunately, as discussed before, the e(t) process is largely composed of the driven response which is temporally correlated.

As a generalization of Equation 19, it can be assumed that the noise process e(t) is not white, but rather is a weakly stationary process. In this case, the model becomes

$$I(k\Delta T) = \sum_{i=1}^{M} a_i \, I[(k - i)\Delta T] + \sum_{i=0}^{P} b_i \, \varepsilon(k - i) \tag{21}$$

where now $\{\varepsilon(t)\}$ is assumed to be white noise, but the input process to the linear filter $\{\alpha_i\}$ is a colored process. Equation 21 is called an autoregressive-moving-average process (ARMA) (Ref. 7). In this case, the spectral density is given by

$$s(f) = \frac{|B(z)|^2}{|A(z)|^2} \tag{22}$$

where A(z) and B(z) are polynomials and

$$z = e^{2\pi i f}$$

In Reference 6 the method of fitting A(z) and B(z) directly from the spectral density is discussed. Numerous methods for fitting ARMA processes exist in time series literature (Ref. 7). They are more stable than the method discussed in Reference 6. Again, none of the methods discussed here are appropriate for the driven response problem because the driven response is a transient that cannot be modeled as a weakly stationary process either.

5. SCOPE OF THIS PAPER

A different time series method, complex demodulation, will be discussed in Section II. Complex demodulation is specifically useful for analyzing transient responses. In Section III, the Prony method and complex demodulation will be compared for a wide range of simulated data responses, including white noise corrupted data and a variety of driven responses. In Section IV, several extensions to the use of complex demodulation will be discussed. In particular, complex demodulation can be used to analyze several sensors, e.g., at several locations on the skin of an aircraft or at several pin locations, simultaneously. Finally, Section V contains the summary and conclusions of this paper.

II. COMPLEX DEMODULATION

Complex demodulation is a very flexible method of analyzing time series data (Ref. 8). The method can best be understood as a time-dependent harmonic analysis. While the method is not as precise as harmonic analysis for analyzing weakly stationary time series or pure harmonics, it is very useful in harmonic analysis of transients. For a detailed discussion of complex demodulation see Reference 9.

Given a process Y(t), construct for some frequency f the new process

$$X(t,f) = e^{-2\pi i f t}\, Y(t) \tag{23}$$

The Fourier transform of the original process {Y} is given by the sample average of the {X} process

$$y(f) = \frac{1}{N} \sum_{k} X(k\Delta T, f) \tag{24}$$

Taking the sample average may be viewed as the most restrictive low pass filter possible. (Allowing only DC to pass, y(f) is a constant with respect to time.) If a less restrictive low pass filter were used on the process {X(t,f)}, a smooth but time-dependent function {x(t,f)}, which would correspond to a time-dependent Fourier transform, would be obtained. The process {x(t,f)} is called the complex demodulate of {Y(t)}.

To understand the flexibility and generality of complex demodulation, first suppose that the process contains a perturbed periodic component

$$Y(t) = R(t) \cos[2\pi\gamma t + \phi(t)] \tag{25}$$

where R(t) is a slowly changing amplitude and $\phi(t)$ a slowly varying phase. The aim of complex demodulation is to estimate R(t) and $\phi(t)$. For any frequency f, form

$$X(t,f) = Y(t)\, e^{-2\pi i f t}$$

$$= R(t) \cos[2\pi\gamma t + \phi(t)]\, e^{-2\pi i f t}$$

$$= R(t)\,\frac{1}{2}\left[e^{2\pi i\gamma t+i\phi(t)} + e^{-2\pi i\gamma t-i\phi(t)}\right] e^{-2\pi ift}$$

$$= \frac{1}{2}\,R(t)\left[e^{2\pi i(\gamma-f)t+i\phi(t)} + e^{-2\pi i(\gamma+f)t-i\phi(t)}\right] \qquad (26)$$

If the frequency γ is near to f, then the $(\gamma - f)$ term will represent a low frequency, while $(\gamma + f)$ will represent a high frequency. If $X(t,f)$ then is passed through a low pass filter, which allows frequencies near zero to pass while filtering out higher frequencies, the resulting complex demodulate will be

$$x(t,f) = \frac{1}{2}\,R(t)\,e^{2\pi i(\gamma-f)t+i\phi(t)} \qquad (27)$$

To obtain this estimate then, it is only necessary to have an initial estimate f such that $(f - \gamma)$ is within the bandwidth of the filter.

It is immediately clear the $R(t)$ is estimated by the magnitude of the complex demodulate and the phase $\phi(t)$ can be estimated by its argument

$$\arg x(t,f) = 2\pi(\gamma - f)t + \phi(t) \qquad (28)$$

If γ is sufficiently close to f, an estimate of $\phi(t)$ is obtained. If ϕ is known to be constant in some time interval, or even known to have a zero trend, then linear regression can be used on the phase function, $\arg x(t,f)$ to estimate $2\pi(\gamma - f)$ and correct the estimate of γ.

The generalization to more than one frequency

$$Y(t) = \sum_{i=1}^{M} R_i(t)\cos[2\pi\gamma_i + \phi_i(t)] \qquad (29)$$

is straightforward. As long as the frequencies γ_i are spread further apart than the bandwidth of the filter, each may be considered a separate problem. This is identical to harmonic analysis where the component of each harmonic is analyzed separately. Here it is seen that harmonic analysis is more precise than complex demodulation because low pass filters of bandwidth π/N are obtainable. What is gained is the fact that the complex demodulation analysis is time dependent.

Consider next the SEM case, a damped sinusoid

$$Y(t) = c\, e^{-\alpha t} \cos(2\pi\gamma t + \phi)$$

$$= \frac{ce^{-\alpha t}}{2}\left[e^{2\pi i\gamma t + i\phi} + e^{-2\pi i\gamma t - i\phi}\right]$$

$$= \frac{ce^{i\phi}}{2} e^{-\alpha t + \pi i\gamma t} + \frac{ce^{-i\phi}}{2} e^{-\alpha t - 2\pi i\gamma t} \qquad (30)$$

This is the same model as Equation 3 only with M = 2 and the two roots being a complex conjugate pair. Then the residue satisfies

$$c_1 = \overline{c}_2$$

$$= \frac{c}{2}\cos(\phi) + i\,\frac{c}{2}\sin(\phi) \qquad (31)$$

and the complex frequency satisfies

$$s_1 = \overline{s}_2$$

$$s_1 = \overline{s}_2 = -\alpha + 2\pi i\gamma \qquad (32)$$

In this case, the magnitude of the complex demodulate satisfies

$$\ln(|x(t,f)|) = \ln(c/2) - \alpha t \qquad (33)$$

Simple linear regression can then be used to estimate c and α. Also, the phase is defined by

$$\arg x(t,f) = \arctan(\text{Imag}[x(t,f)]/\text{Real}[x(t,f])$$

$$= 2\pi(\gamma - f)t + \phi \qquad (34)$$

which can also be used in a simple linear regression to estimate γ and ϕ.

It should be emphasized that it is not necessary to know γ in advance, but only to be close relative to the bandwidth of the low pass filter. The initial estimates of γ can come from theoretical investigations or from spectral peaks since the spectral density will have a peak of

$$f_o = \sqrt{\gamma^2 - \alpha^2/4} \tag{35}$$

It is also important to note that the complex demodulation in no way requires the data to conform exactly to the natural response as in Equation 3. It will be seen in the analysis of various noise corrupted and driven responses in the next section that the fit or lack of fit of the simple straight lines in the magnitude and phase functions is a superb diagnostic for the model. It is easy to determine the time interval when the driven response (g(t)) has diminished and it is possible to estimate the natural (SEM) response directly. However, it is also possible to estimate the parameters of the natural response during the early (driven) part of the data realization by computing the effect of the driving function on R(t) and ϕ(t). As will be seen, a great advantage of complex demodulation over using Prony's method is that it allows analysis of the data during early time before all transients have decreased. It will also be seen that the low pass filter in complex demodulation succeeds in removing a significant part of the noise and greatly improving its sensitivity to noise. Also, it succeeds in removing driven responses that are not in the immediate frequency range being analyzed.

Finally, it should be noted that complex demodulation estimates the natural frequencies directly. A problem with the Prony method is that estimation errors for a_k can produce even larger errors in the estimation of c_k when solving for the roots of Equation 5. This propagation of errors frequently produces non-physical estimates, roots in the right half plane in particular. The direct estimate of the complex frequency in complex demodulation avoids this problem.

III. COMPARISON OF PRONY AND COMPLEX DEMODULATION

1. SIMPLE MODELS

In this section, the pure damped sinusoid (Eq. 30) will be analyzed with Prony and with complex demodulation. Then the example of a damped sinusoid plus white noise will give a more important comparison of the two methods.

The first model studied was a simple damped sinusoid with frequency 3 MHz and damping constant 0.5×10^6. The data are displayed in Figure 1. The Prony analysis of these data, which is very accurate, is shown in Table 1.

TABLE 1. PRONY ANALYSIS FOR DAMPED SINUSOID

Coefficient	Partial Correlation	Autoregressive Parameter (a_i)
0	1.000000	1.000000
1	.995578	-1.986152
2	-.995012	.995012

Complex Roots			
Number	Root (z_i)	Natural Frequency (s_i)	Frequency (MHz)
1	(0.9931, 0.9387e-01)	(-0.5000, 18.85)	3.0000
2	(0.9931, -0.9387e-01)	(-0.5000, -18.85)	-3.0000

Table 1 contains some terminology common to time series analysis. The partial correlation is the correlation of Y_t with Y_{t+k} when $Y_{t+1}, \ldots, Y_{t+k-1}$ have been accounted for. This is a valuable term for estimating M. The autoregressive parameter is $\{a_i\}$. Figure 2 is the spectral density of the data, which, of course, peaks very close to 3 MHz. To demonstrate the use of Equation 34 in refining the frequency, a very wide miss of 3.25 MHz was used in a complex demodulation. Shown in Figure 3 is the phase plot from which a slope of -1.57×10^6 is obtained. Using Equation 34 and setting the slope equal to:

$$-1.57 \times 10^6 = 2\pi(\gamma - 3.25 \text{ MHz}) \tag{36}$$

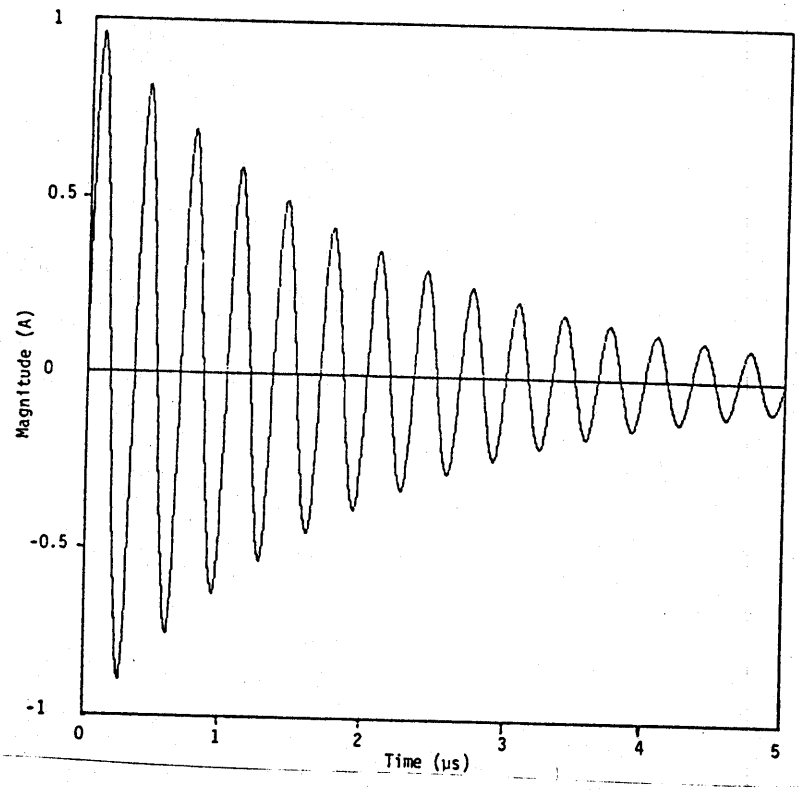

Figure 1. Damped sinusoid, 3 MHz.

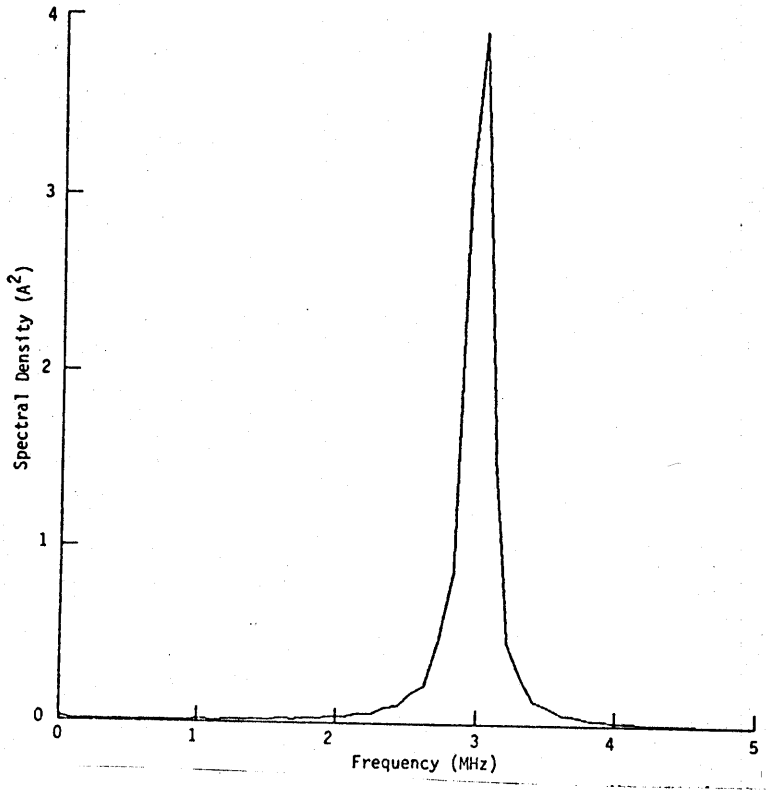

Figure 2. Spectral density of damped sinusoid.

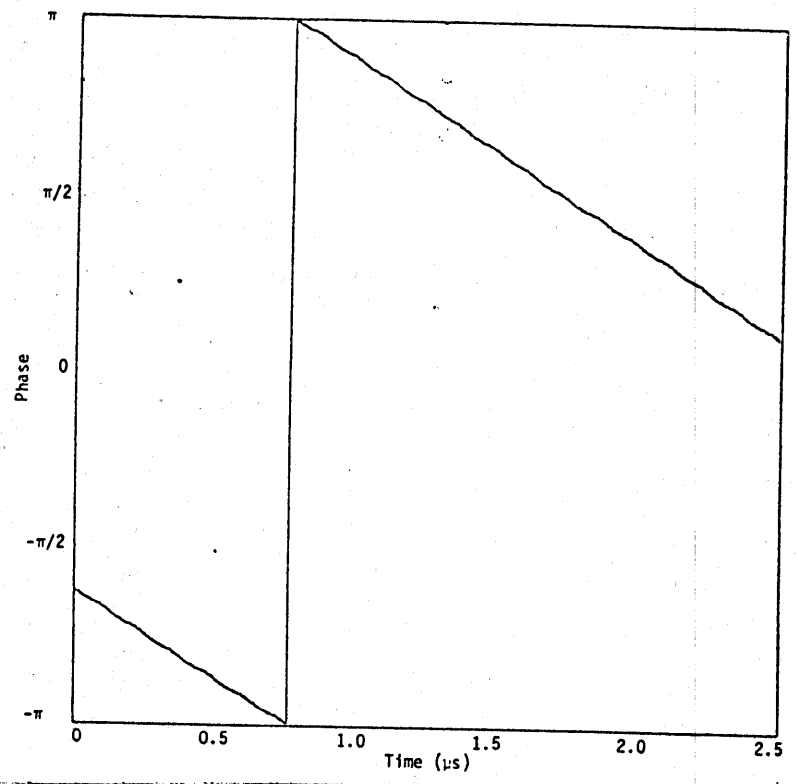

Figure 3. Phase plot of complex demodulation at 3.25 MHz.

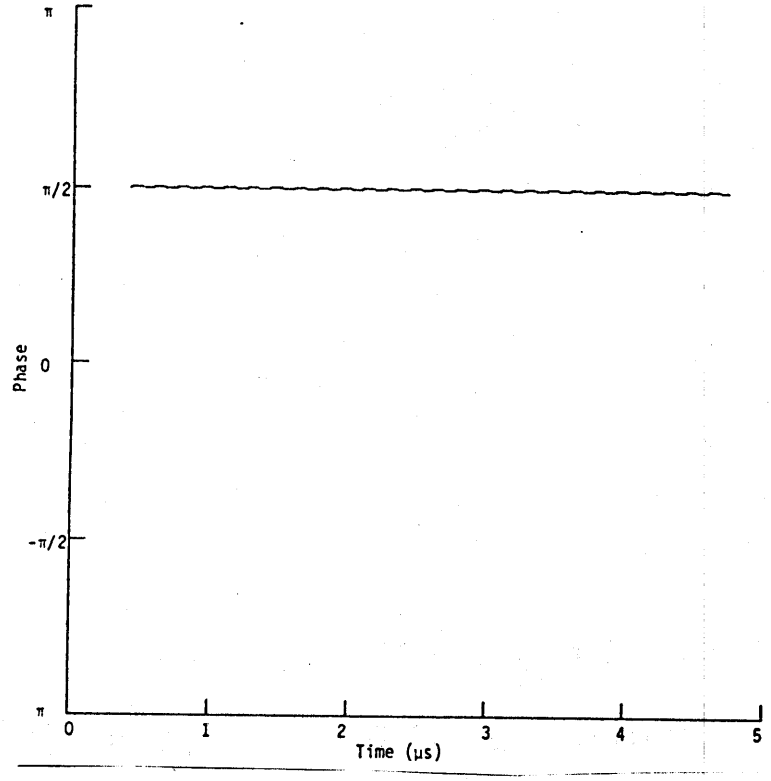

Figure 4. Phase plot of complex demodulation at 3 MHz.

yields 3 MHz as the best estimate of γ. Figure 4 is the phase plot for the analysis at 3 MHz; the slope of the phase is zero. The intercept of the data in Figure 4 was estimated to be -1.5710, which is close to $-\pi/2$, the difference between the sine used and the cosine in the definition of complex demodulation (Eq. 25). Finally, Figure 5 is the magnitude of the complex demodulate, which has an estimated residue of 1.0036 (the true value is 1.00) and a slope (damping factor) of -0.5001×10^6.

The next experiment was to add Gaussian white noise to the damped sinusoid data used in the above paragraph. The damped sinusoid has a residue of 1.00, and the Gaussian noise with standard deviations from 0.001 to 0.1 was added. Table 2 compares the Prony and complex demodulation estimates. As a rough estimate of signal-to-noise (S/N) ratios, let the standard deviation of the signal be 0.5 (the residue of 1.0 is taken as two standard deviations). Then Prony began having difficulty at an S/N of 200, and failed to estimate physically meaningful parameters after an S/N of 50. At an S/N of 5, complex demodulation was still estimating reasonably well.

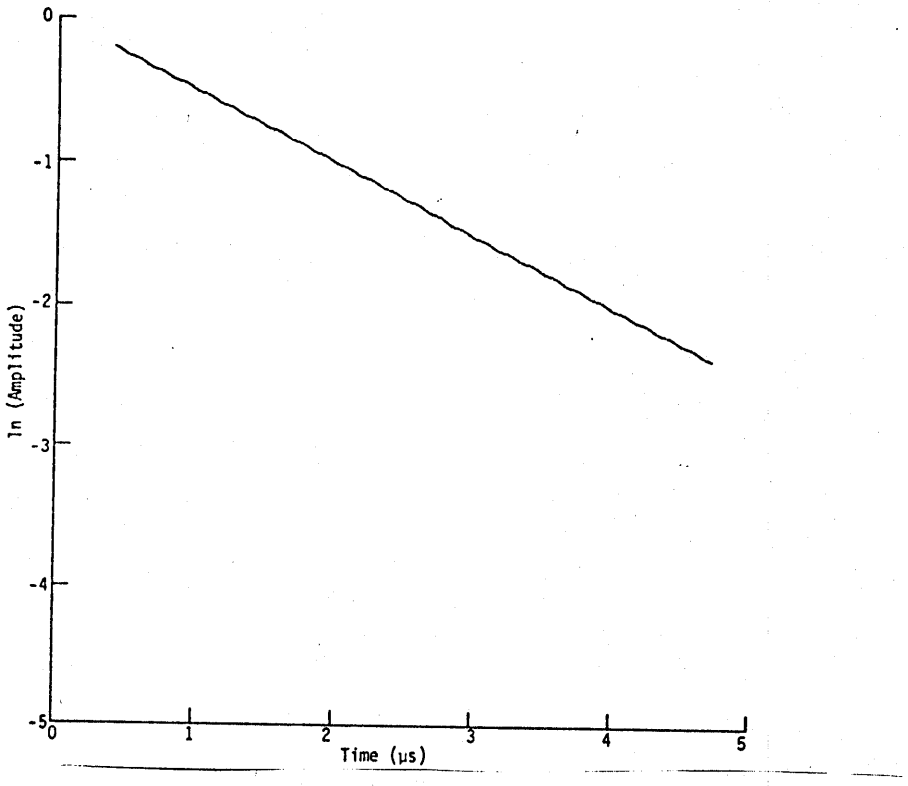

Figure 5. Magnitude plot of complex demodulation at 3 MHz.

TABLE 2. PRONY AND COMPLEX DEMODULATION DAMPED SINUSOID PLUS WHITE NOISE

Deviation Noise Standard	Prony		Complex Demodulation	
	Damping Factor ($\times 10^6$)	Frequency (MHz)	Damping Factor ($\times 10^6$)	Frequency (MHz)
0.0	-.5000	3.0000	-.5001	3.0000
0.001	-.8833	3.0015	-.5003	3.0000
0.0025	-2.746	2.9905	-.5008	3.0000
0.005	-8.129	2.7939	-.5012	3.0003
0.01	REAL ROOTS		-.5004	3.0000
0.05	REAL ROOTS		-.4954	3.0000
0.10	REAL ROOTS		-.5114	3.0028

Figure 6 is the damped sinusoid plus noise with a noise standard deviation of 0.10 (the last row of Table 2). Figure 7 is the spectral density of the data. Figure 8 is the phase plot of the complex demodulate at 3.0000. The slight slope in Figure 8, which is hardly visible, resulted in an estimate of 3.0028 MHz. Finally, the magnitude of the complex demodulation at 3 MHz is shown in Figure 9.

The performance of complex demodulation in the above experiment was not surprising. The low pass filter used in complex demodulation actually removes most of the white noise and allows the analysis to experience signal-to-noise ratios greatly in excess of what is present over all frequencies. In fairness to the Prony method, the modifications discussed in Section I.4 would have performed much better than Prony itself. This has not been followed as the real point is still that the driven response in Equation 1 is neither white nor stationary, but rather a transient. The point to be made here is the natural insensitivity of the complex demodulation method to noise.

2. DRIVEN MODELS

To study the response of the Prony method and complex demodulation to more realistic problems, several experiments are conducted to study driven responses. A very simple system of a simple LRC circuit is used to get the response of a damped harmonic. The response is then given by the solution to

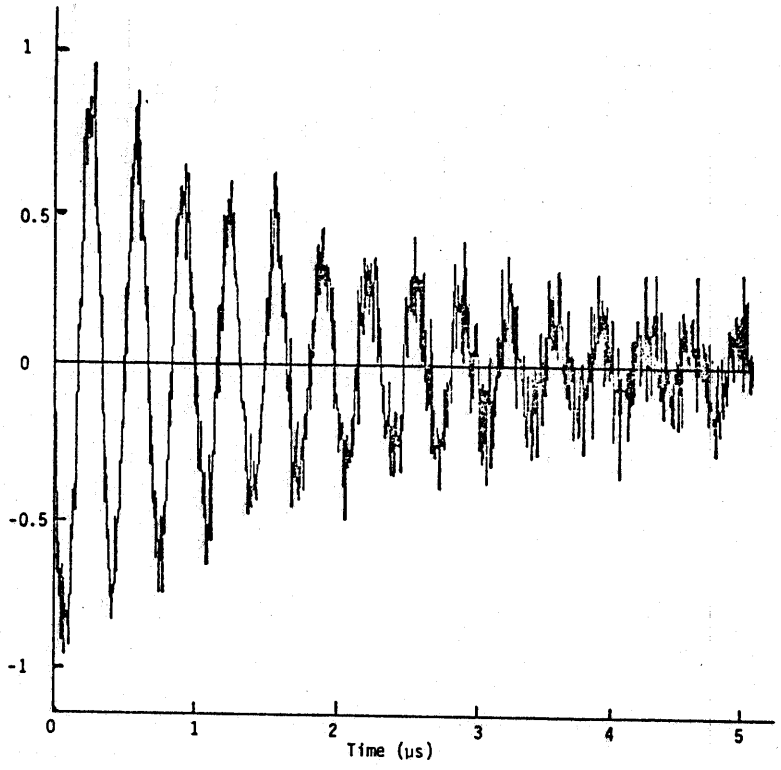

Figure 6. Damped sinusoid (3 MHz) plus white noise (σ = .10).

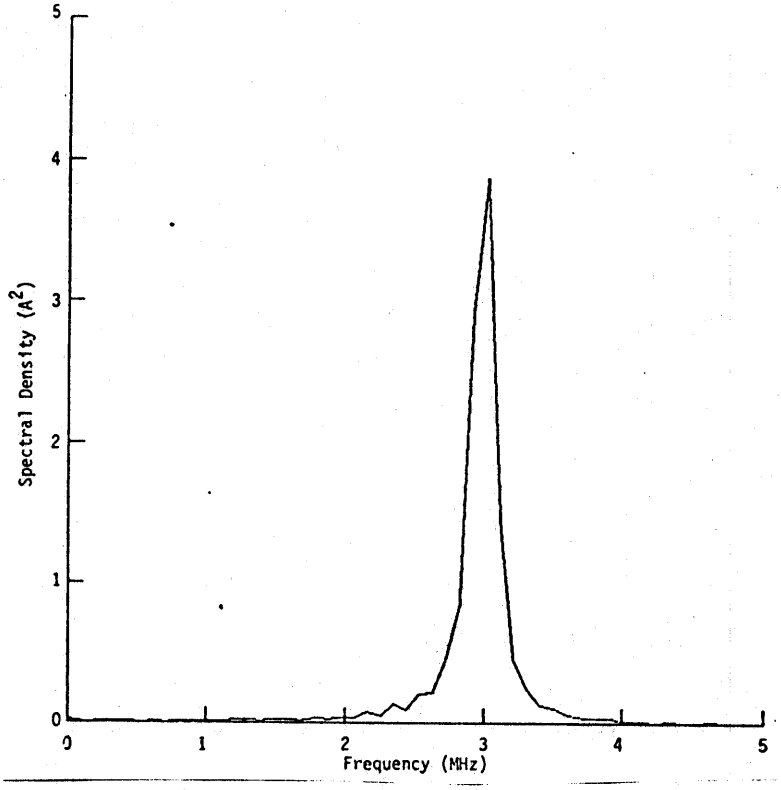

Figure 7. Spectral density for damped sinusoid plus noise.

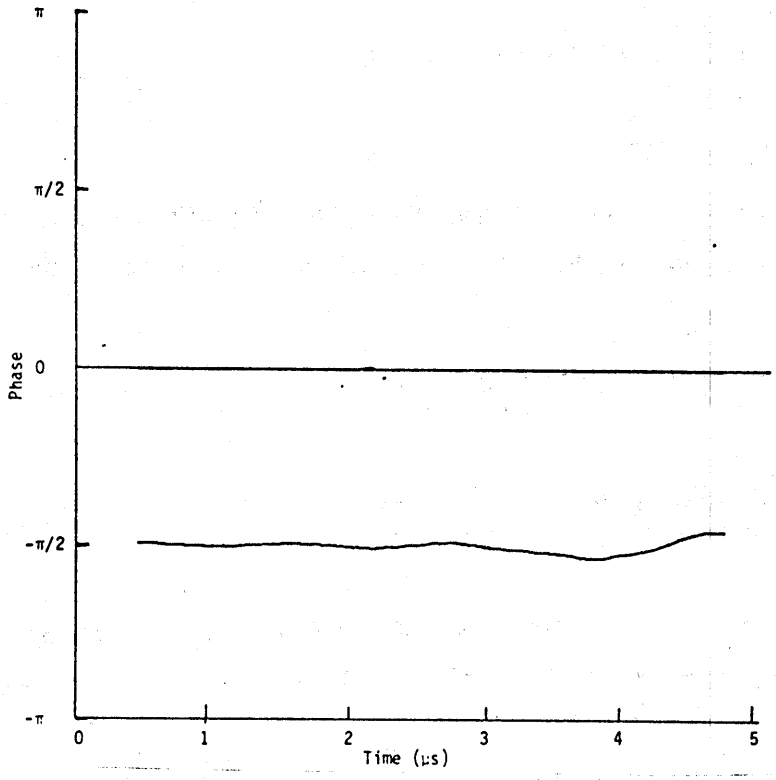

Figure 8. Phase plot for complex demodulation at 3 MHz.

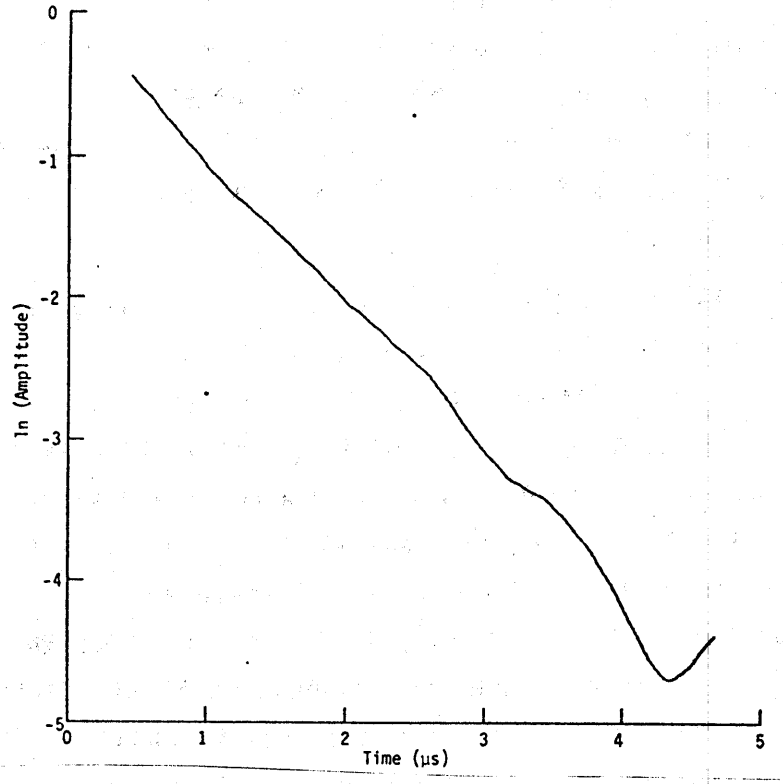

Figure 9. Magnitude plot for complex demodulation at 3 MHz.

$$I(t) = \int_0^t F(t - u)\, e^{-\alpha u} \sin(2\pi\gamma u)\, du \qquad (37)$$

for any forcing function $F(t)$.

The first experiment was to drive the LRC circuit with a damped sinusoid. A well known relationship for the Laplace transform of the solution in this particular case is that

$$X(s) = \frac{\omega_1}{(s + \alpha)^2 + \omega_1^2} \frac{\omega_2}{(s + \beta)^2 + \omega_2^2}$$

$$= \frac{As + B}{(s + \alpha)^2 + \omega_1^2} + \frac{Cs + D}{(s + \beta)^2 + \omega_2^2} \qquad (38)$$

That is, the solution to the damped harmonic oscillator, driven by a damped sinusoid, can be represented as the sum of two damped sinusoids with the same complex frequencies.

The LRC circuit was taken to have a resonance at 3 MHz with a damping factor of -0.5×10^6, and the driving function was taken to be a damped sinusoid with a resonance of 4 MHz and a damping factor of -1.5×10^6. The data are displayed in Figure 10, and the spectral density of the data is displayed in Figure 11. The spectral density shows the two peaks at 3 MHz and 4 MHz. It is interesting to note that the output peak (3 MHz) is greater than the input peak (4 MHz). Table 3 is the result of the Prony method, which, as expected, is very accurate.

The complex demodulation analysis of this case is very illustrative of the method. Figures 12 and 13 are the phase plots at 3 and 4 MHz, respectively. Figure 12, which is at the resonant frequency of the circuit, illustrates the presence of beating frequencies for the driving frequency (the wave in the phase plot is at 1 MHz). The damped beating frequency has a slope of zero, so the non-zero phase, as in Equation 28, can still be used to adjust the frequency. Figure 13, however, shows a very different aspect. The driving function quickly subsides ($\alpha = -1.5 \times 10^6$, or $Q = 8.4$ as compared to $Q = 18.9$ for the driven circuit). This is seen by the beating in the first cycle, as expected, followed by information to shift the analysis down 1 MHz to 3 MHz. The magnitudes of the beating in Figures 12 and 13 reflect the magnitudes of

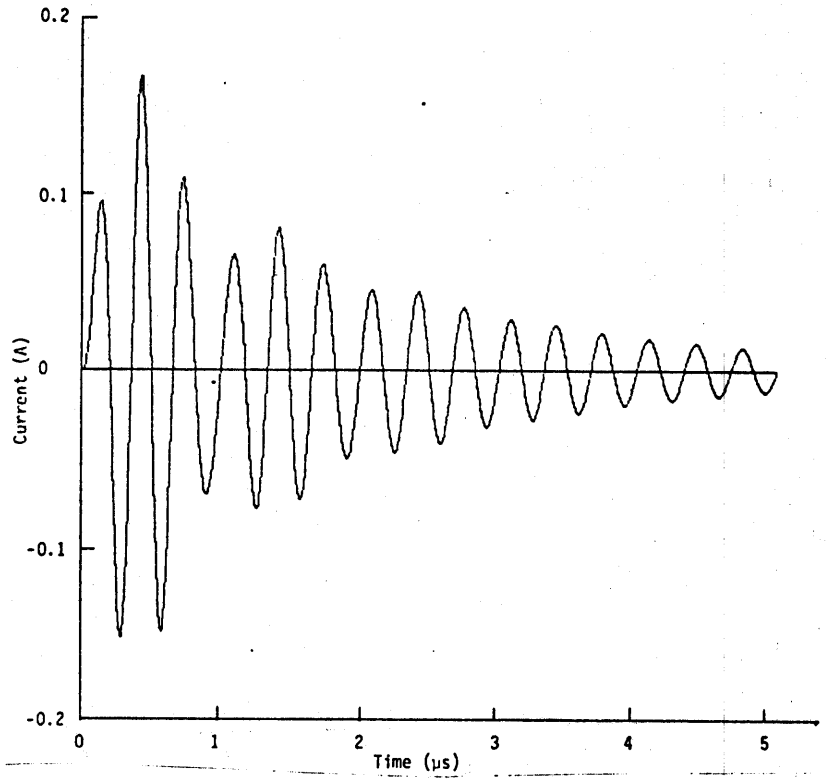

Figure 10. 3 MHz resonant circuit driven at 4 MHz.

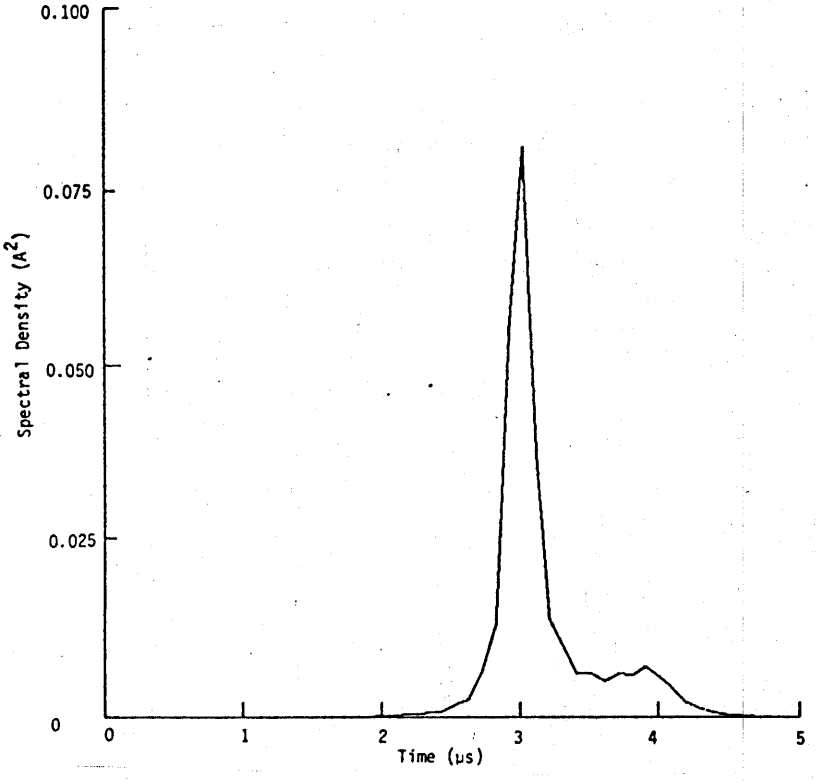

Figure 11. Spectral density, 4 MHz resonant device driven at 3 MHz.

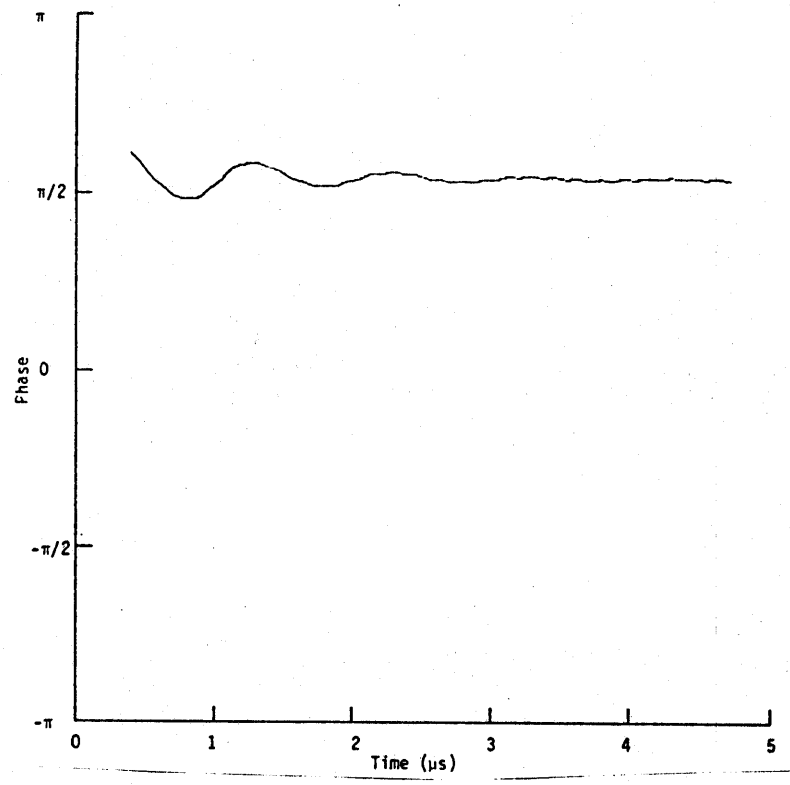

Figure 12. Phase plot for complex demodulation at 3 MHz.

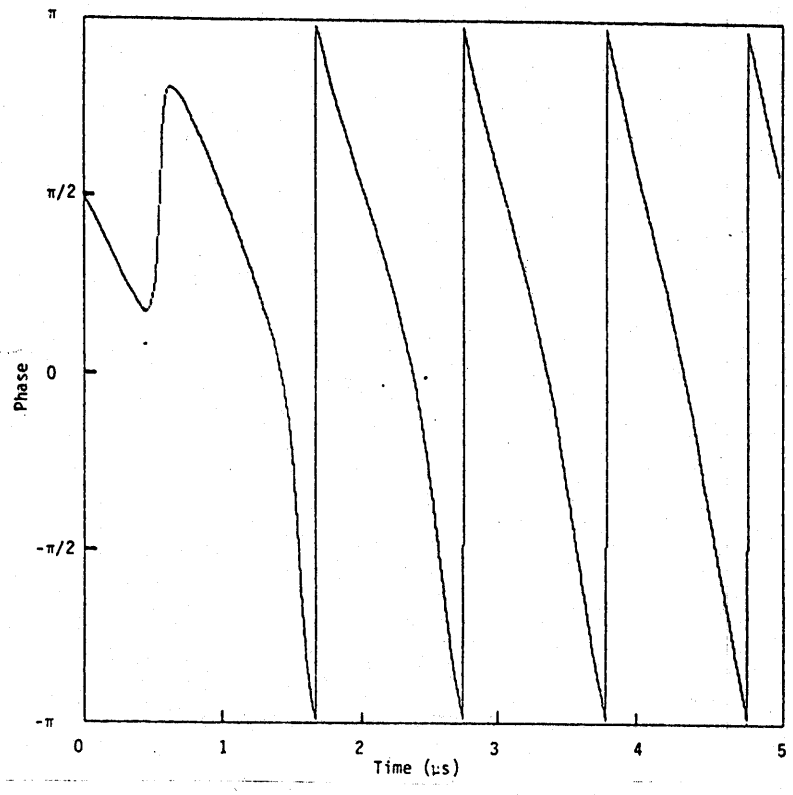

Figure 13. Phase plot for complex demodulation at 4 MHz.

TABLE 3. PRONY ANALYSIS FOR DAMPED SINUSOID DRIVING FUNCTION

Coefficient	Partial Correlation	Autoregressive Parameter (a_i)
0	1.000000	1.000000
1	0.995056	-3.955555
2	-.999677	5.891659
3	0.992414	-3.916162
4	-.980198	0.980198

Complex Roots

Number	Root (z_i)	Natural Frequency (s_i)	Frequency (MHz)
1	(0.9847, 0.1244)	(-1.500, 25.13)	4.0000
2	(0.9847, -0.1244)	(-1.500, -25.13)	-4.0000
3	(0.9931, 0.9387e-01)	(-0.5000, 18.85)	3.0000
4	(0.9931, -0.9387e-01)	(-0.5000, -18.85)	-3.0000

the spectral peaks in Figure 11. Figure 14 displays the magnitude plot for the complex demodulation at 3 MHz. Again, the ln R(t) is not a simple straight line, as is the case in Equation 30. However, the superimposed damped sinusoid at the beating frequency (1 MHz) has zero slope, and so the damping coefficient can still be estimated from the slope of the magnitude. As will be discussed later in this paper, the complex demodulation method lends itself well with a total systems approach to analyzing the data in that knowledge of the theoretical models can help understand the skin currents and information about the skin currents in turn can be utilized in understanding the pin currents.

The simple relationship given by Equation 38 for a damped oscillator driven by a damped sinusoid does not hold when the driving function is altered. To illustrate this, data were first generated for a damped oscillator driven by a double exponential function. This result would be somewhat typical of the response of the skin of an aircraft to an actual EMP event. The response to the first oscillator (the skin) was then used to drive a second damped oscillator. The result is representative of the effect of an actual electronic component driven by the skin response.

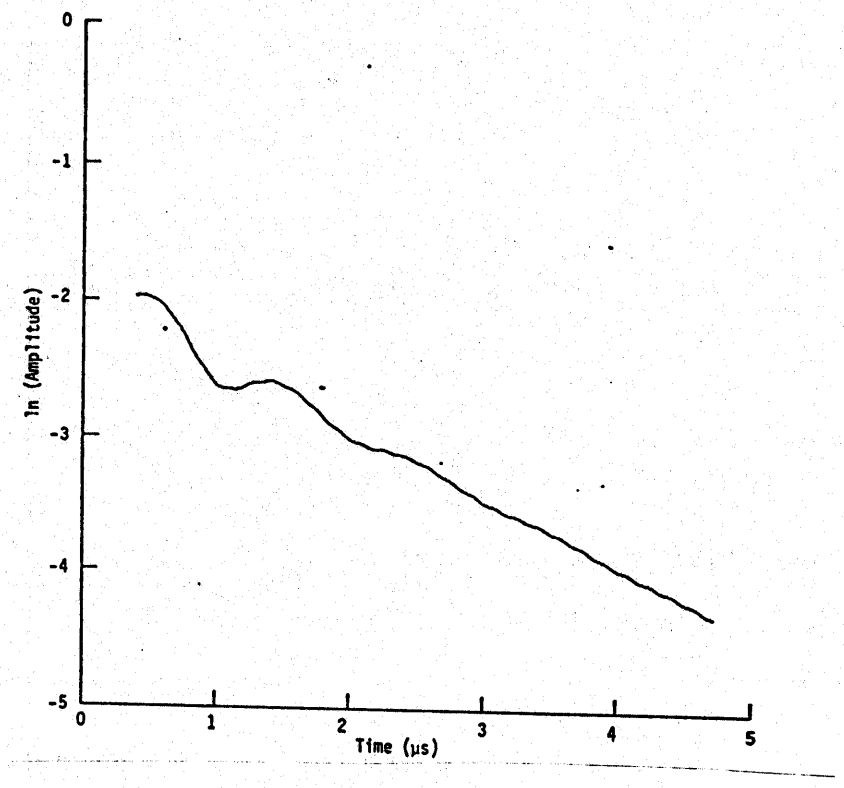

Figure 14. Magnitude plot for complex demodulation at 3 MHz.

The first part of the experiment was to simulate the skin response. The skin was taken to have a resonance of 3 MHz with a damping coefficient of -1.5×10^6. The double exponential driving function,

$$F(t) = e^{-\beta_1 t} - e^{-\beta_2 t} \tag{39}$$

with $\beta_1 = 4 \times 10^6$ and $\beta_2 = 4.76 \times 10^8$ was used as input. The response is displayed in Figure 15 and its spectral density in Figure 16. The overshoot phenomena in Figure 15 creates a very low frequency response as the system settles back to oscillating about the origin. This is seen by the low frequency peak in Figure 16 that makes the data appear to have a real root to the

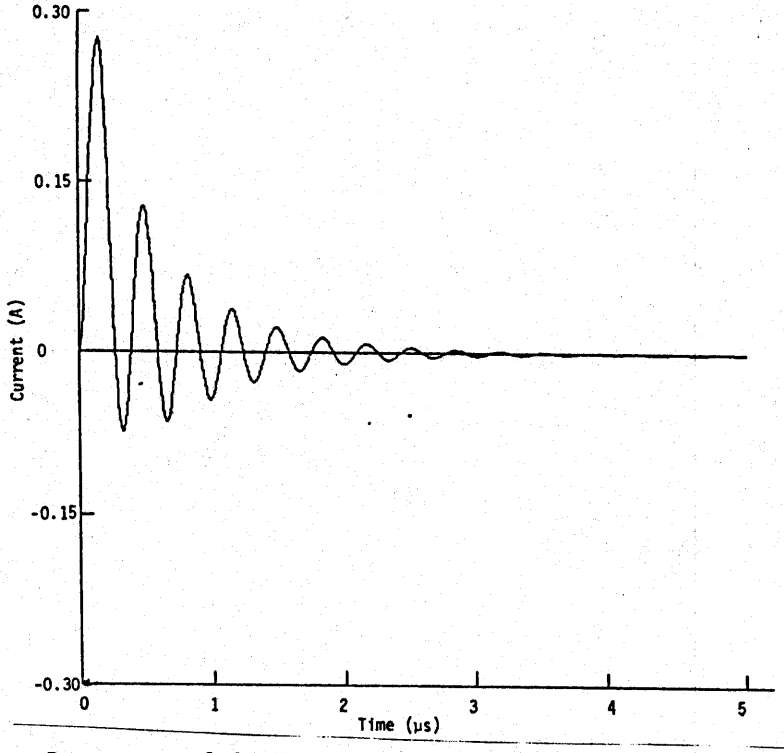

Figure 15. Response of 3 MHz resonant circuit to double exponential drive.

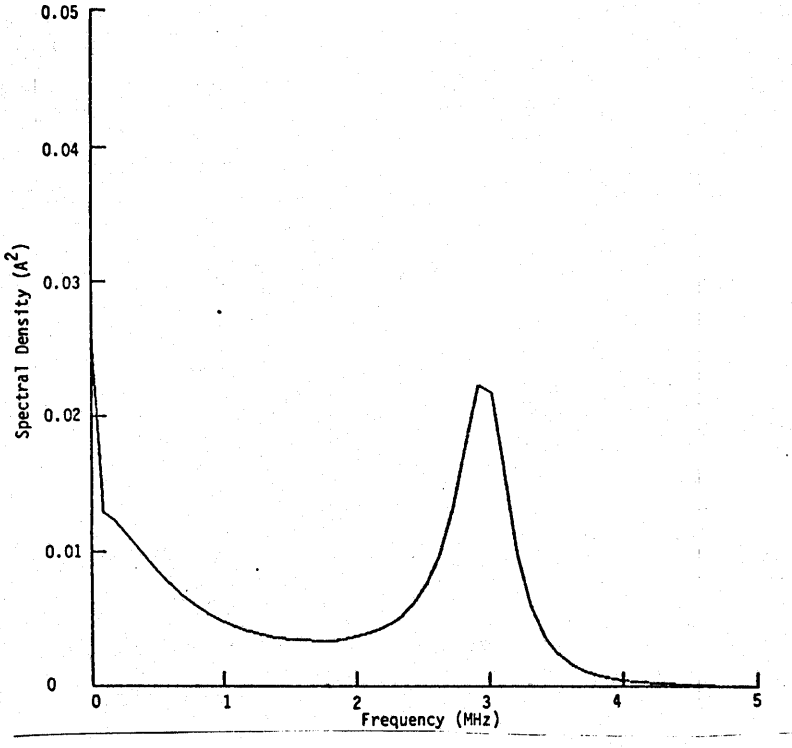

Figure 16. Spectral density of response to double exponential drive.

Prony method. This real root is not a physically real aspect of the skin, but rather this is a good example of how the driven response of Equation 1 generates nonphysical phenomena in Prony analyses. The results of the Prony analysis are shown in Table 4.

The complex demodulation method now really begins to show its merit. It is able to analyze data that do not follow the form of Equation 3 exactly, yet still get reasonable results. The double exponential driving function had very little effect on complex demodulation because such a small part of its energy was in the frequency band about 3 MHz passed by the low pass filter. Figure 17 displays the phase plot, and Figure 18 displays the magnitude plot for the complex demodulation at 3 MHz. The complex demodulation method estimated the residue to be 0.2147, the damping factor α = 1.5002 x 10^6, the frequency f = 3.0000 MHz, and the phase ϕ = 3.0522.

TABLE 4. PRONY ANALYSIS OF SKIN RESPONSE

Coefficient	Partial Correlation	Autoregressive Parameter (a_i)
0	1.000000	1.000000
1	0.997449	-2.965037
2	-0.997920	2.939336
3	0.974167	-0.974167

Complex Roots

Number	Root (z_i)	Natural Frequency (s_i)	Frequency (MHz)
1	(0.9899, 0.9413e-01)	(-1.137, 18.96)	3.0179
2	(0.9899, -0.9413e-01)	(-1.137, -18.96)	-3.0179
3	(0.9853, 0.0000e+00)	(-2.961, 0.0000e+00)	0.0000

The next step was to use the simulated skin data (Fig. 15) as the forcing function to a second harmonic oscillator. The second oscillator, representing circuitry inside the aircraft, was taken to have a resonance of 4 MHz and a damping factor of 0.5 x 10^6. The result of this experiment is displayed in

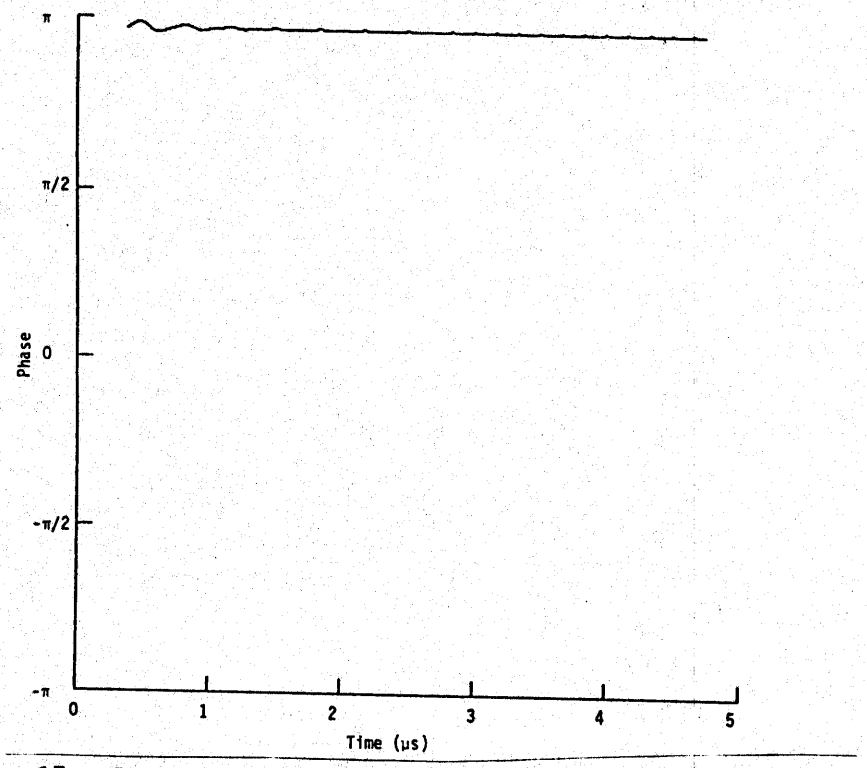

Figure 17. Phase plot for complex demodulation at 3 MHz.

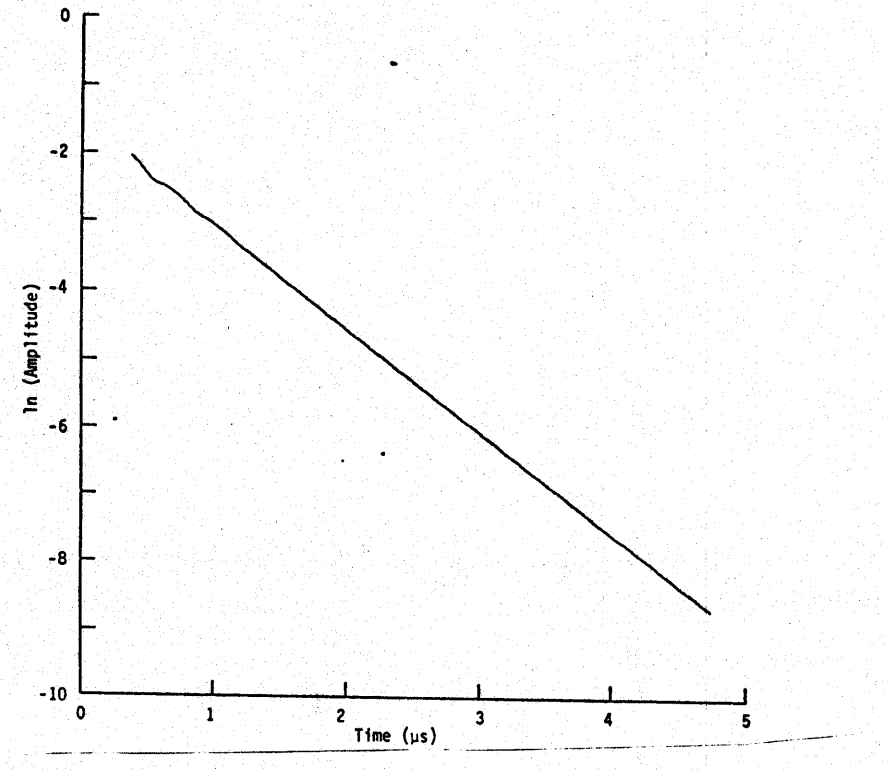

Figure 18. Magnitude plot for complex demodulation at 3 MHz.

Figure 19. Since the data displayed in Figure 15 better resemble a damped sinusoid than a double exponential, it would be reasonable to expect the Prony method to perform better on the simulated pin data. As Table 5 shows, the Prony method did still worse.

The result of the complex demodulation analysis is very similar to the previous driven response. The spectral density of the simulated pin data is shown in Figure 20. The phase plot of the complex demodulation at 4 MHz is displayed in Figure 21 and the magnitude plot in Figure 22. The complex demodulation method estimated the residue to be 0.0046, the damping factor $\alpha = -0.5262 \times 10^6$, the frequency 4.0025 MHz, and the phase $\phi = -.2131$. The 1 MHz beating frequency is also visible in Figures 21 and 22.

The final driven response experiment was intended to simulate the effect of time delays and spatial phase shifts that would be created as the result of the several points of entry in the aircraft skin located in different parts of the aircraft. The data were generated to be the output of a damped oscillator with a resonance of 4 MHz and a damping coefficient of -0.5×10^6. The forcing function was a damped sinusoid with a frequency of 3.9 MHz and a damping coefficient of -1.5×10^6, minus twice the same forcing function delayed

TABLE 5. PRONY ANALYSIS OF SIMULATED PIN DATA

Coefficient	Partial Correlation	Autoregressive Parameter (a_i)
0	1.000000	1.000000
1	0.994354	-3.977720
2	-0.999074	5.952666
3	0.996922	-3.971992
4	-0.997116	0.997116

Complex Roots

Number	Root (z_i)	Natural Frequency (s_i)	Frequency (MHz)
1	(0.9925, 0.1205)	(-0.3877e-01, 24.17)	3.8467
2	(0.9925, -0.1205)	(-0.3877e-01, -24.17)	-3.8467
3	(0.9963, 0.6927e-01)	(-0.2500, 13.88)	2.2095
4	(0.9963, -0.6927e-01)	(-0.2500, -13.88)	-2.2095

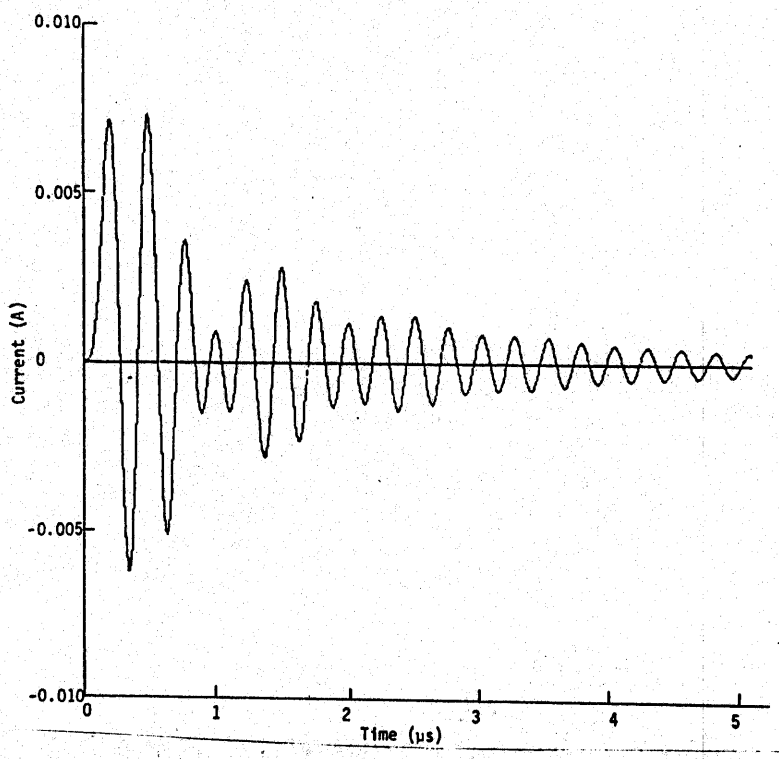

Figure 19. Response of 4 MHz resonant circuit to simulated skin current.

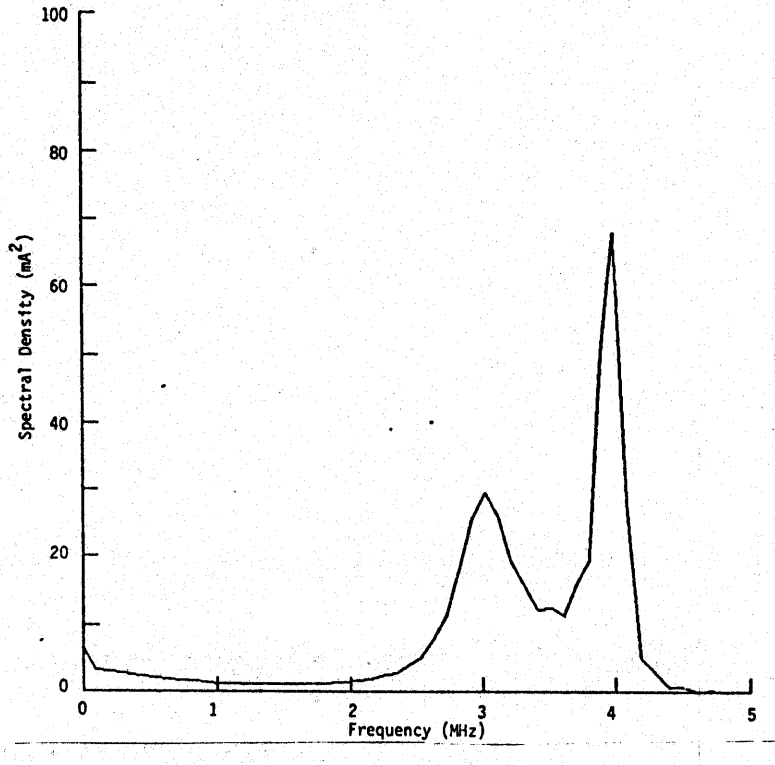

Figure 20. Spectral density of simulated pin response.

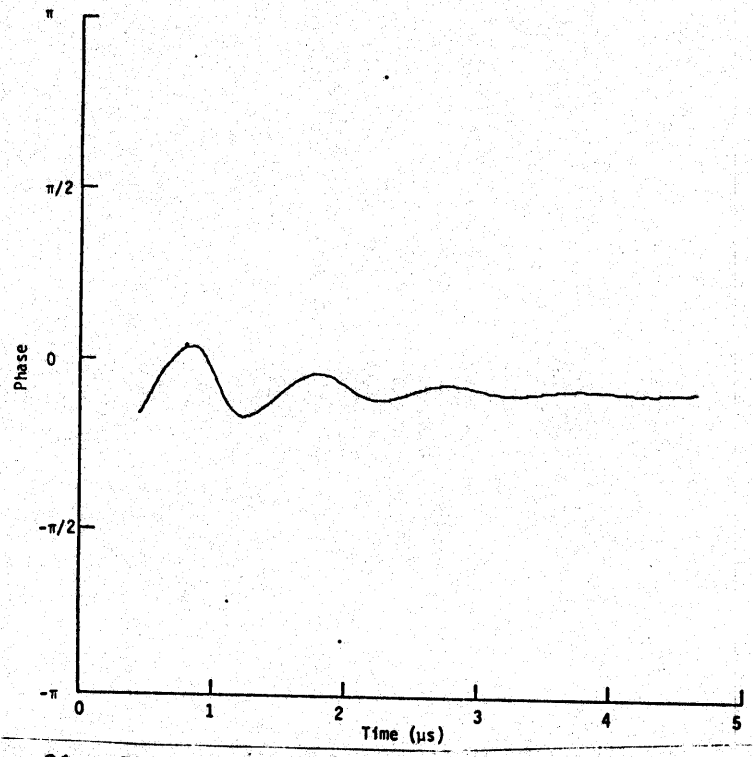

Figure 21. Phase plot for complex demodulation at 4 MHz.

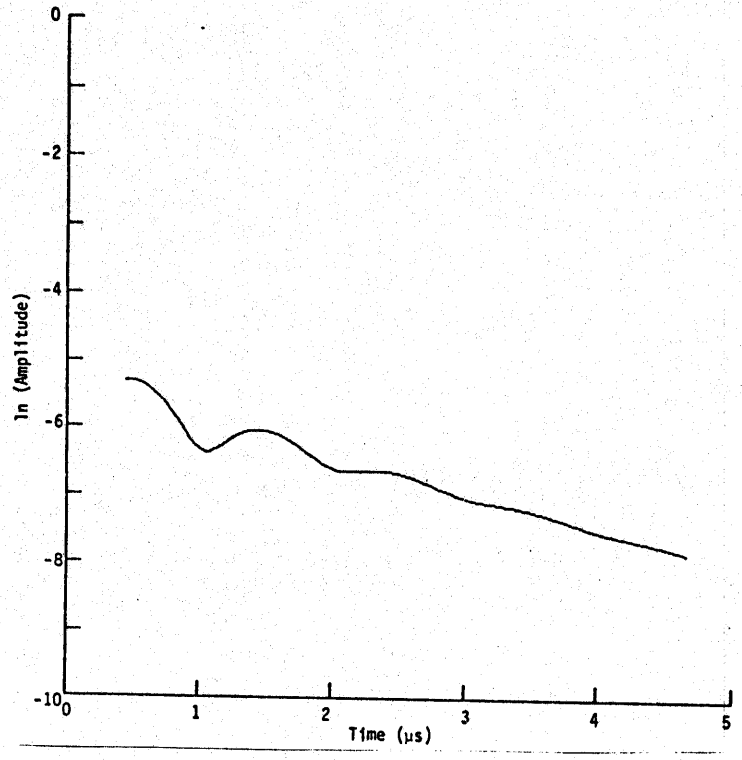

Figure 22. Magnitude plot for complex demodulation at 4 MHz.

20 ns, plus twice the same forcing function delayed 40 ns, minus the same forcing function delayed 60 ns. The data are displayed in Figure 23 and, except for the abrupt change of direction in the first cycle, they appear exactly as if they have been driven simply with one damped sinusoid at 3.9 MHz.

Again it seems that the Prony method should work as well as it did in Table 3. In fact, however, the Prony method performed very poorly. Knowing that there should be two pairs of roots, Table 6 gives the results of the Prony analysis. The presence of the partial correlation greater than one in magnitude is evidence of the fact that all partial correlations having magnitude less than one is a sufficient, but not a necessary, condition for all roots to be inside the unit circle. As a result of the partial correlation, the usual method of deciding where to stop adding roots selects two roots. This analysis, presented in Table 7, does in fact have a root in the right half plane.

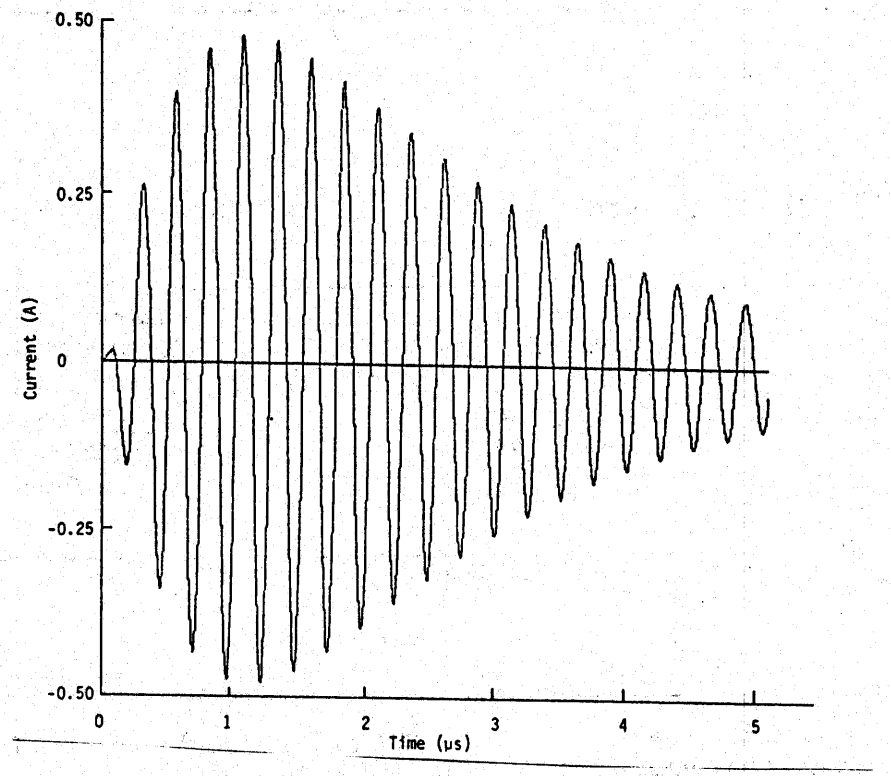

Figure 23. Response to delayed drives.

TABLE 6. PRONY ANALYSIS WITH FOUR ROOTS

Coefficient	Partial Correlation	Autoregressive Parameter (a_i)
0	1.000000	1.000000
1	0.992281	-3.894798
2	-1.000038	5.720057
3	0.990046	-3.754031
4	-0.929063	0.929063

Complex Roots

Number	Root (z_i)	Natural Frequency (s_i)	Frequency (MHz)
1	(0.9557, 0.1292)	(-7.247, 26.87)	4.2767
2	(0.9557, -0.1292)	(-7.247, -26.87)	-4.2767
3	(0.9917, 0.1244)	(-0.1112, 24.95)	3.9714
4	(0.9917, -0.1244)	(-0.1112, -24.95)	-3.9714

TABLE 7. PRONY ANALYSIS WITH TWO ROOTS

Coefficient	Partial Correlation	Autoregressive Parameter (a_i)
0	1.000000	1.000000
1	0.992281	-1.984511
3	-1.000038	1.000038

Complex Roots

Number	Root (z_i)	Natural Frequency (s_i)	Frequency (MHz)
1	(0.9923, 0.1244)	(0.3771e-02, 24.94)	3.9689
2	(0.9923, -0.1244)	(0.3771e-02, -24.94)	-3.9689

The complex demodulation method continued to respond well. The spectral density is displayed in Figure 24. The phase plot and magnitude plot for the complex demodulation analysis at 4 MHz are displayed in Figures 25 and 26. The key to Prony's problem is revealed in these plots. After the delayed signals with alternating signs stopped arriving, the response was liberated and did actually increase in magnitude briefly. Using the entire data record in Figure 26 to estimate the residue and the damping would underestimate both (although the slope of the data in Figure 26 would still be negative giving roots in the left half of the plane). However, using that portion of the data where the phase (Fig. 25) has stabilized, Figure 26 gives an estimate of 1.1 for the residue and $\alpha = -0.5 \times 10^6$ for the damping coefficient.

3. ANALYSIS OF PIN CURRENTS FOR TRESTLE TESTS OF AN AIRCRAFT SYSTEM

The Prony method has been applied to skin currents with some success. However, the Prony method has not been very successful in analyzing pin currents. The experiments discussed in III.1 and III.2 provided ample evidence for the Prony method not being appropriate for analyzing pin responses. Pin data from a Trestle test, which was analyzed using complex demodulation, is now discussed in detail. This exercise demonstrates the ability of complex

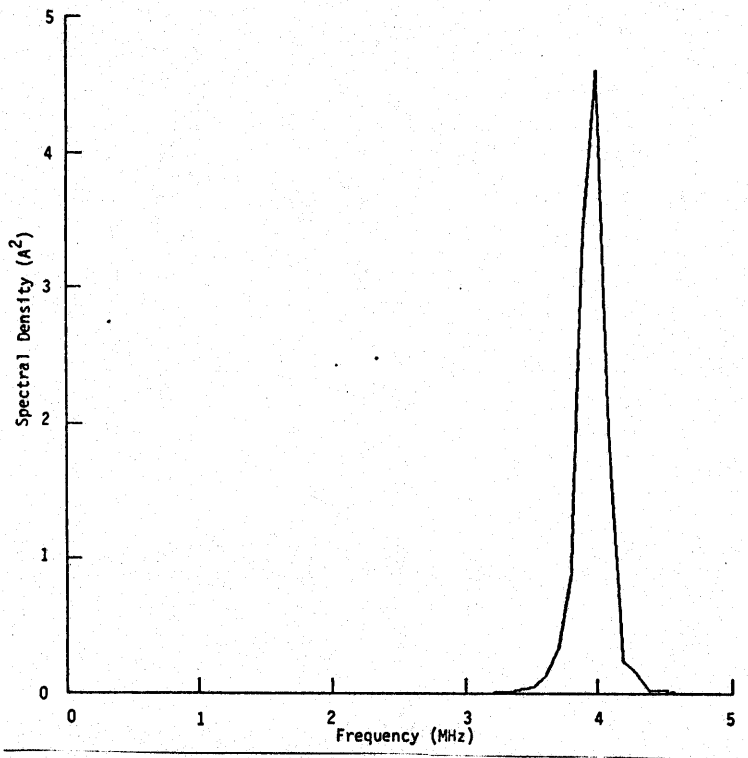

Figure 24. Spectral density for response to delayed drives.

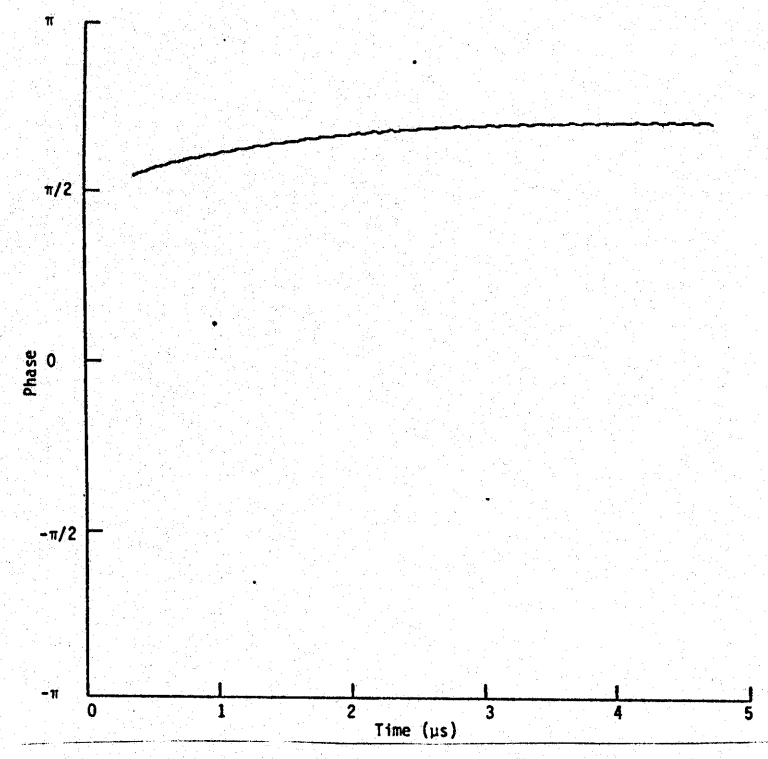

Figure 25. Phase plot for complex demodulation at 4 MHz.

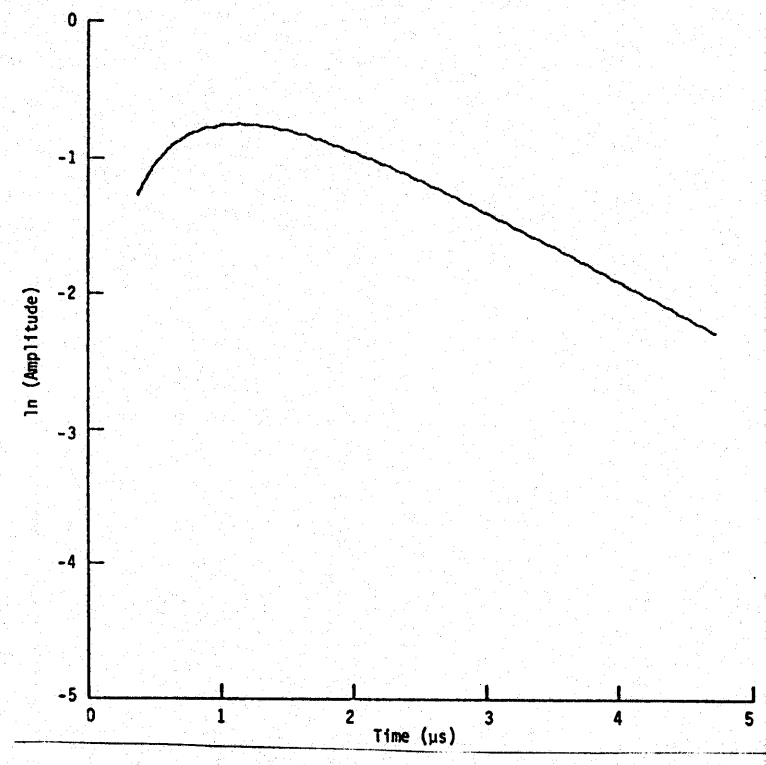

Figure 26. Magnitude plot for complex demodulation at 4 MHz.

demodulation to analyze very difficult data. The data collected at the same pin for four other shots were also analyzed using complex demodulation. This analysis of the pin currents was used in Reference 10 to compare the energy predicted by a single damped sinusoid, using f = 1 MHz, Q = 24, and the residue equal to the peak current, with a more comprehensive analysis of the data. The results of this analysis are summarized in Table 8.

These analyses are in a sense blind since no information is available on field or skin response. The complex demodulation method is most convincing when used in a total systems approach where the information from the previous level of analysis is used to implement any new analysis. While such an approach is desirable and possible with complex demodulation, this analysis demonstrates that it is not necessary.

TABLE 8. DAMPED SINUSOID ANALYSIS OF TRESTLE SAMPLE AIRCRAFT DATA

Shot No.	Frequency (MHz) γ_i	Amplitude (A) $\lvert c_i \rvert$	Damping ($\times 10^{-6}$) α_i
1	1.95	0.27	-0.65
	3.65	0.31	-1.73
	5.50	0.63	-1.1
	8.90	0.79	-1.6
2	3.30	0.25	-0.89
	4.40	0.28	-0.89
	5.40	0.72	-1.1
	8.20	0.84	-0.88
3	3.30	0.17	-0.82
	4.40	0.14	-0.93
	5.70	0.24	-1.2
	8.80	0.05	0.83
4	1.70	0.43	-0.66
	4.30	1.12	-1.6
	5.80	0.94	-1.3
	7.70	0.21	-1.3
5	1.80	0.33	-0.61
	3.90	0.94	-1.6
	5.70	0.78	-1.2
	7.50	0.12	-1.0

Figure 27 is a plot of the current observed at the example pin. It displays many features similar to the examples of the last two subsections. Figure 28 is a plot of the spectral density of the data. The complex demodulation analyses of the peaks at 2, 4, and 5.4 MHz are presented. As will be immediately obvious from the numerous driven examples in III.2, the small peak just below 4 MHz looks familiar.

Figures 29 to 32 are phase and magnitude plots for the analyses at 2 and 5.4 MHz. The plots are as expected with the only surprise being the phase shifts due to the practice of time-tying the data. The method estimated a residue of 0.27, a damping coefficient of $\alpha = -0.65 \times 10^6$, and a phase of $\phi = 0.21$ at 1.95 MHz. It also estimated a residue of 0.63, a damping coefficient of $\alpha = -1.1 \times 10^6$, and a phase of $\phi = 1.73$ at 5.5 MHz.

As suspected from Figure 28, the analysis around 4 MHz was more interesting. The method settled on the small peak at 3.65 MHz. The phase plot and magnitude plot for the complex demodulation at 3.65 MHz are shown in Figures 33 and 34, respectively. The beating frequency of 0.33 MHz, apparent in Figures 33 and 34, implies a driving function in the neighborhood of 3.98 MHz (the large peak in Figure 28). There is a spectral peak between 3.85 and 4 MHz in a large number of pin currents from the aircraft Trestle test, and it is a logical guess that there will be a fundamental mode in this neighborhood for the aircraft. Analysis of skin currents to confirm this would be productive. For comparison, the data were band-pass filtered with a filter centered at 3.65 MHz and a 0.75 MHz bandwidth. These data are presented in Figure 35; its similarities to Figures 10 and 19 are noteworthy.

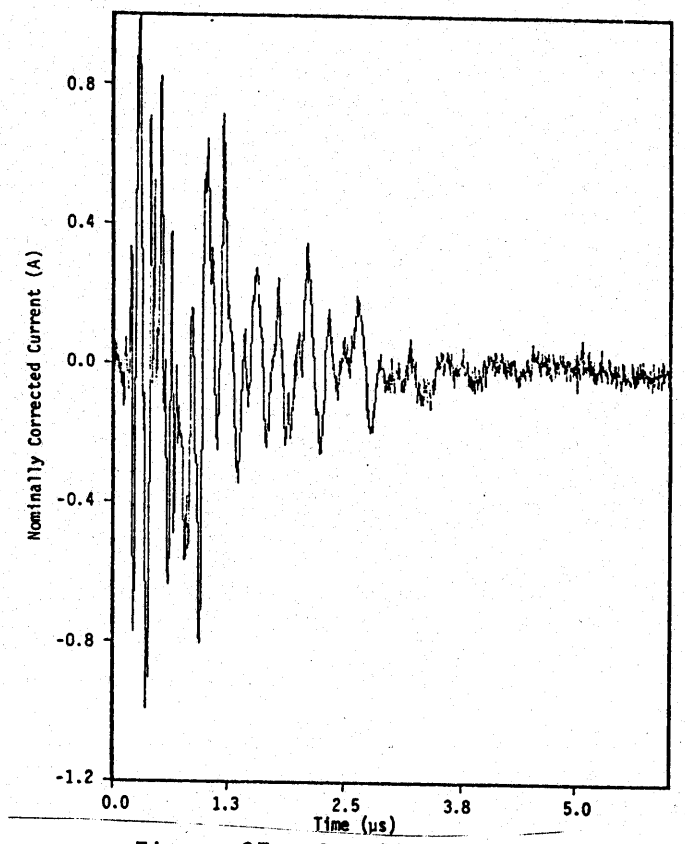

Figure 27. Sample waveform.

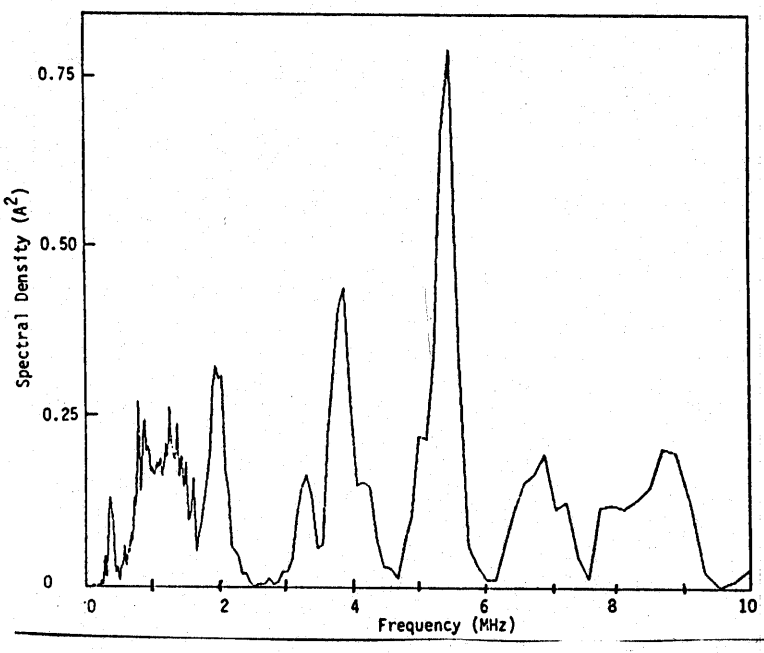

Figure 28. Spectral density for sample waveform.

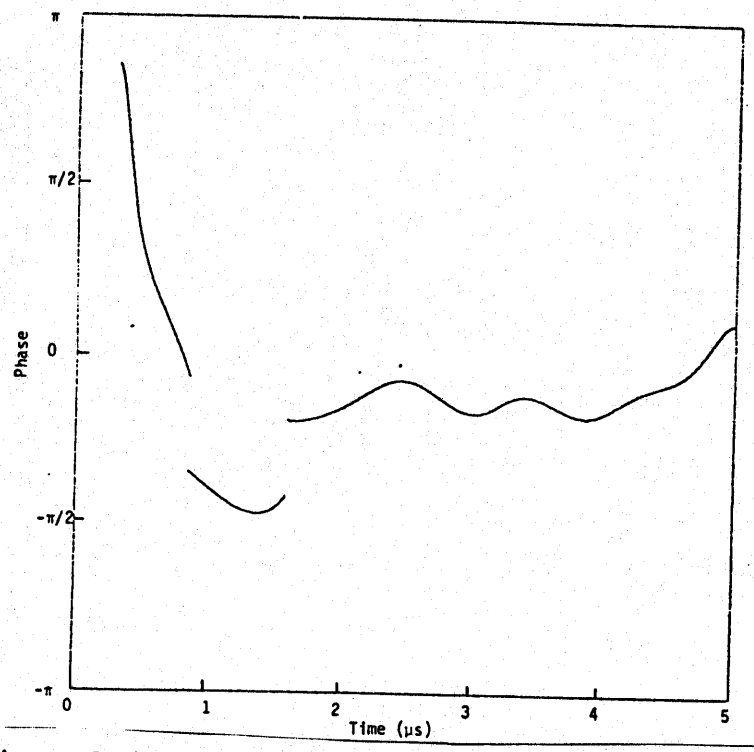

Figure 29. Phase plot for 1.95 MHz, 1980 Trestle test.

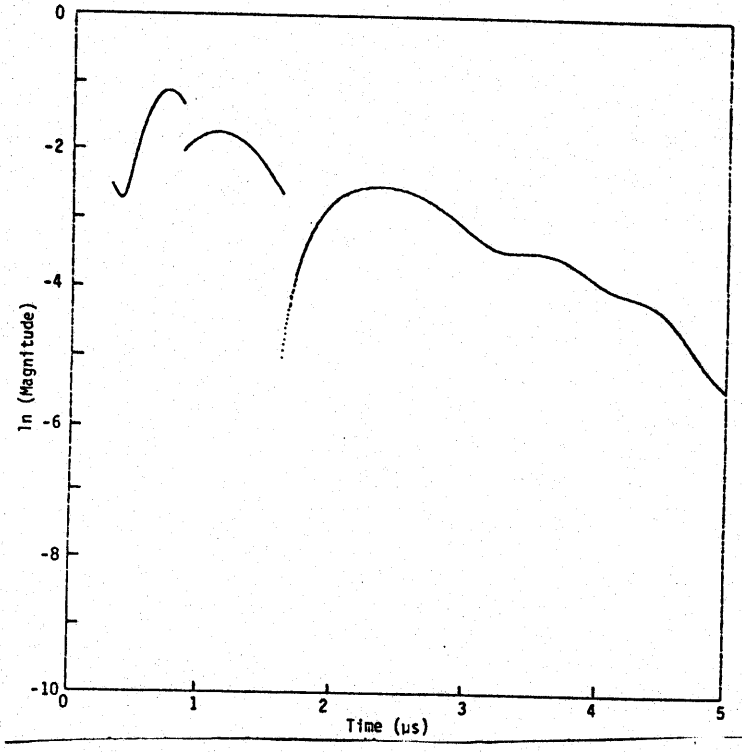

Figure 30. Magnitude plot for 1.95 MHz, 1980 Trestle test.

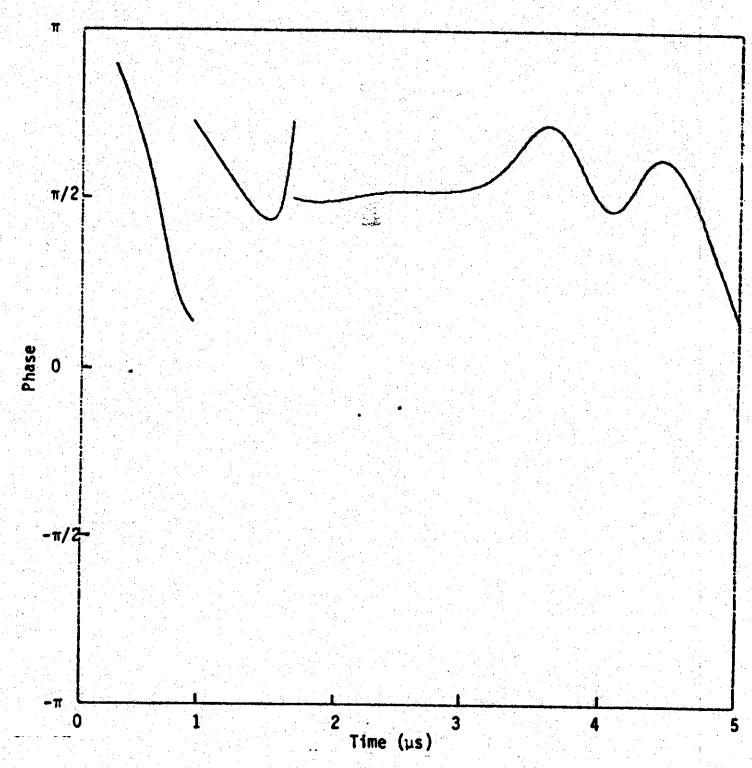

Figure 31. Phase plot for 5.5 MHz, pin #1047, shot #5089, 1980 Trestle test.

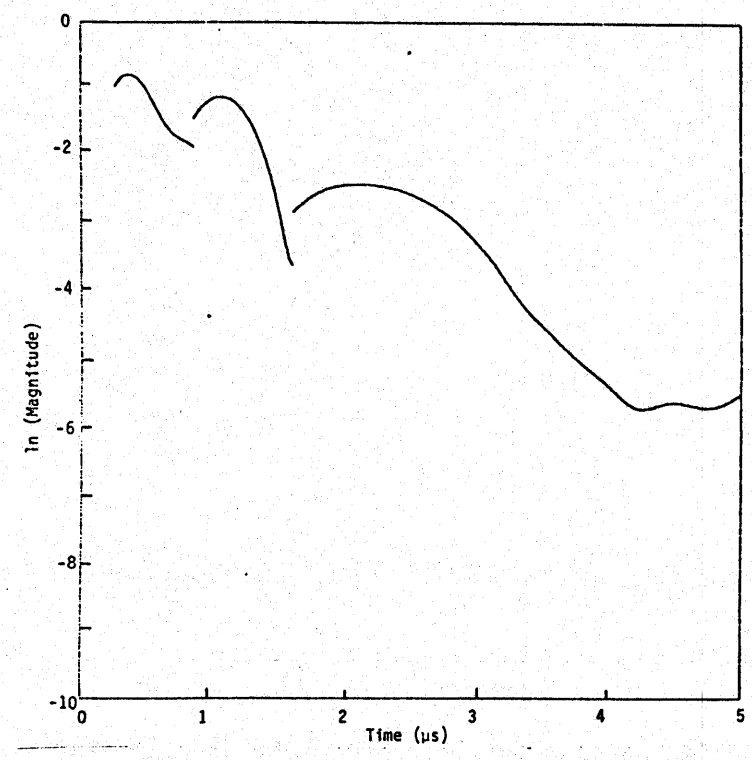

Figure 32. Magnitude plot for 5.5 MHz, pin #1047, shot #5089, 1980 Trestle test.

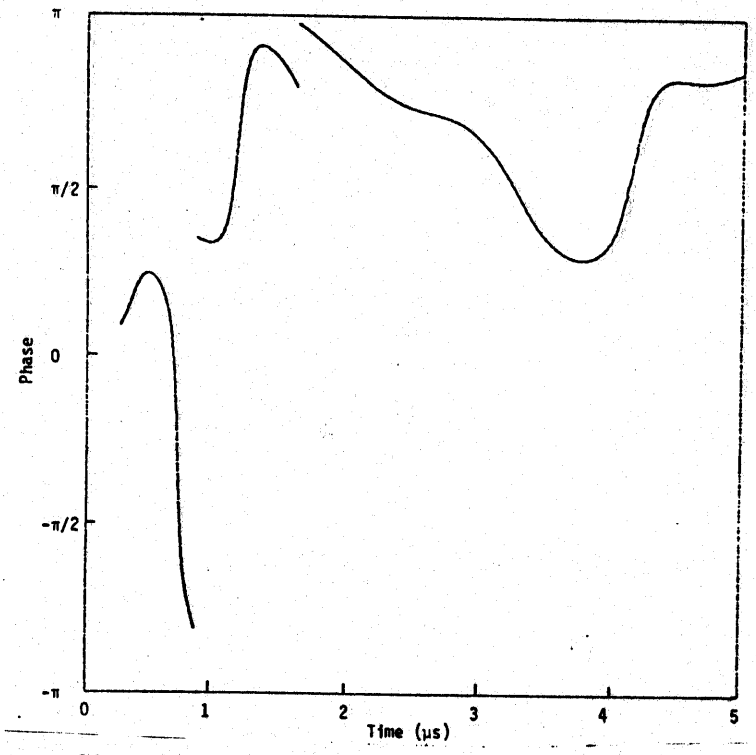

Figure 33. Phase plot for 3.65 MHz, 1980 Trestle test.

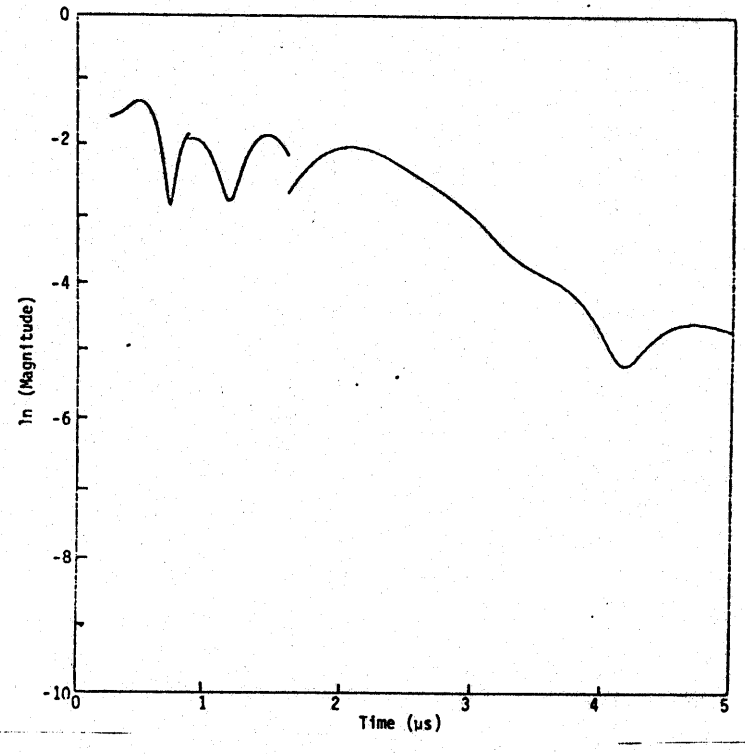

Figure 34. Magnitude plot for 3.65 MHz, 1980 Trestle test.

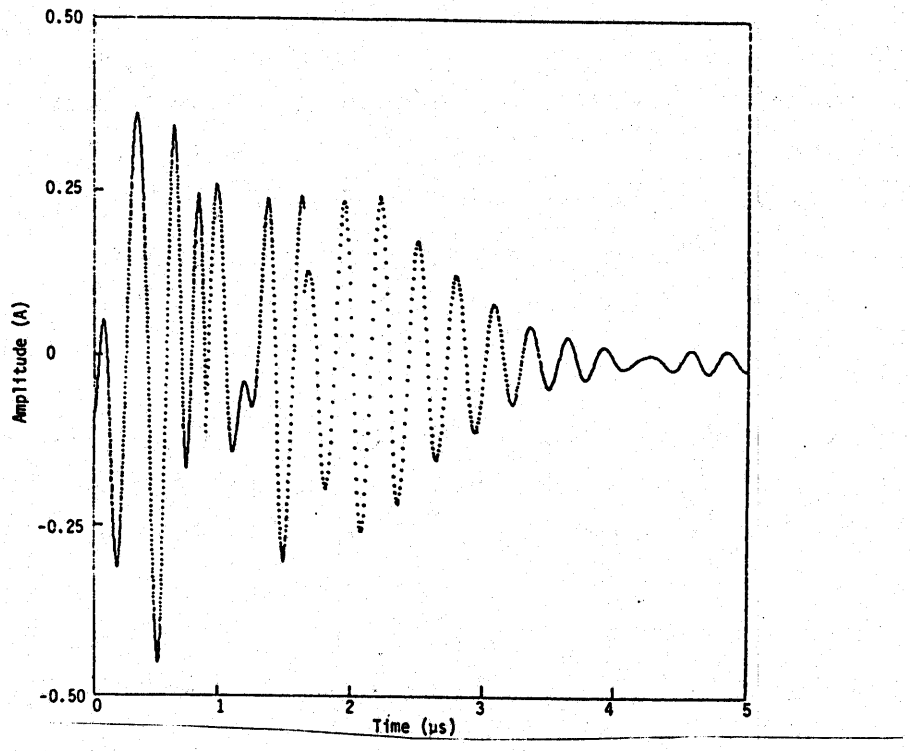

Figure 35. Complex demodulate, bandpass filtered at 3.65 MHz with 0.75 MHz bandwidth.

IV. EXTENSIONS TO COMPLEX DEMODULATION

1. LINEAR MODELS

The use of least squares regression with straight lines, and even with polynomials, is commonly understood. The method of linear least squares is in fact much more general. This section contains a discussion of linear models that are useful for analyzing complex demodulation output.

A general linear model is defined to be any question of the form

$$Y = \sum_{i=1}^{p} \beta_i X_i + \varepsilon \tag{40}$$

where Y is the observed output variable, the $\{X_i\}$ are p independent variables which are known beforehand (not random variables, but input constants), and ε is the random error. The parameters $\{\beta_i\}$ are the linear coefficients to be estimated.

Various assumptions can be made for the error, ε. These result in different properties of the least squares estimator. The only assumption needed for least squares to be sensible is that the expected value of ε be zero,

$$E[\varepsilon] = 0 \tag{41}$$

This assumption is adequate to make the least squares estimators unbiased. In I.3, it was mentioned that the estimators for Prony, using least squares, and for the autoregressive parameters can be biased. The use of previous values of Y for X values is a deviation from the above assumption about the independent variables, $\{X_i\}$, and the unbiased property of least squares estimators does not apply. The assumption of homogeneity, that the variance of ε exists and is constant throughout the data set, is important from a pracatical point of view because least squares regression is known for its extreme sensitivity to large values of the residual.

Polynomial models are an important example of the model in Equation 40. That is, let

$$Y = \beta_1 + \beta_2 t + \beta_3 t^2 + \ldots + \beta_p t^{p-1} + \varepsilon \tag{42}$$

The independent variables in Equation 40 are simply powers of the independent variable t.

Another important class of independent variables consists of the so-called design, or dummy, variables. Assume, in the EMP case, that sensors are located at s locations on the surface of the aircraft. For a single mode, the complex frequency should be the same at each sensor, but the residue and phase will change from sensor to sensor. A linear model that would allow analyzing all of the data from the s sensor to estimate the common frequency from the phase data of the complex demodulation of the data sets would be

$$y = \sum_{i=1}^{s} \beta_i X_i + 2\pi(\gamma - f)t + \varepsilon \tag{43}$$

where

$$X_i = \begin{cases} 1 \text{ if from sensor } i \\ 0 \text{ otherwise} \end{cases}$$

and y is the phase data from the complex demodulation. Using this mode, β_1 to β_2 will be the phase of each sensor, while β_{s+1} is the frequency correction. Another model simmilar to Equation 43 would use sensor 1 as a reference and estimate the phase shift of every other sensor relative to sensor 1. This model would be given by

$$y = \beta_1 + \sum_{i=1}^{s} \beta_i X_i + 2\pi(\gamma - f)t + \varepsilon \tag{44}$$

Corresponding to the analysis of phase in Equations 43 and 44, the magnitude information can be used to estimate the residue for each sensor while estimating one damping coefficient common to all sensors. Analagous to Equation 43, this model would be given by

$$y = \sum_{i=1}^{s} \beta_i X_i + \beta_{s+1} t + \varepsilon \tag{45}$$

where now y is the magnitude information from the complex demodulations and $-\beta_{s+1} = \alpha$ the common damping coefficient.

The above linear models can be repeated with pin data collected at several pins. This analysis will allow investigation of frequencies that seem to pervade the interior of the aircraft by appearing at many pins.

The concept where complex demodulation seems most powerful is the one using the above models in a total systems analysis of the aircraft. A study of pin currents using models like those in Equations 43 to 45 can allow a thorough knowledge of the skin response to the EMP wave. Analysis at the next layer, say the pin level interior to the aircraft, could use Equation 44 for the phase information of a complex demodulation at one of the exterior sensor locations to a given pin. This information could be extremely useful in identifying POE locations. A similar analysis using Equation 45 can be used to assess the transfer attenuation or POE degradation.

2. AUTOMATED ANALYSIS

The process for analyzing transient data described up to this point has been very analyst intensive. This is not really necessary since the deviations from the nominal damped sinusoid model are not extreme. A very simple method of having a program identify the spectral peaks and perform complex demodulation analyses simply by fitting straight line models for the data from 2 to 4 μs has been used. This was done for the data collected at the same pin from five different shots during 1980 and 1982 Trestle tests. The analyses for one of the five shots displayed in Figures 29 to 34, were a part of that analysis.

It is possible to implement numerous adaptive algorithms that will produce a computer code capable of rather sophisticated analysis. Recent statistical literature is replete with robust regression algorithms that iteratively reweight the data according to its validity with the model. There are also L_1 codes that minimize the median deviation rather than the squared deviations as least squares does. These codes could make excellent seed codes for initiating a sophisticated analysis.

An important aspect of any codes devised to analyze the complex demodulation data is the ability to pass uneventful data, and know when (and how) to handle data that do not conform to expectations. For example, hard copies of plots of phase and magnitude can be archived for those realization/frequency combinations where the straight line fit is bad. Also, standard deviations

for the straight line fits could be saved with the SEM parameters in a data base so that the remote user could get immediate indication of the value of the fit.

Perhaps the most dangerous aspect of the Prony method is the ability to obtain an answer whether or not the answer is appropriate. Roots in the right half plane are the only indication of difficulty.

V. SUMMARY AND CONCLUSIONS

Complex demodulation is a very flexible tool for analyzing transient data. It is particularly useful in estimating the parameters of an SEM analysis. The method is applicable during the early (driven) part of the response where it can give useful diagnostic information on the nature of the driven response. The method is very stable in the presence of noise, and the method is applicable for a wide range of possible models so that data which do not follow a damped sinusoid model can still be analyzed reliably. It also can analyze data collected simultaneously from several sensors, constraining the common complex frequency parameters to be consistent. The method also estimates the SEM parameters directly, removing the circumstances where the Prony method gives nonphysical estimates.

Complex demodulation can make very valuable contributions to the System Level Evaluation of Electromagnetic Tests (SLEET) data base. First, as input to the data base it can be used as a reliable and trustworthy tool for compacting the data realizations. It has been proven on pin data which tends to be very noisy and difficult to analyze. Second, complex demodulation would allow sophisticated analysis of system level data which SLEET makes available, but which other analysis tools cannot effectively utilize.

The complex demodulation method can be used to integrate theoretical results and actual data in ways that have not been done previously. The method is capable of analyzing the data with no prior information about the structure of the data, but it is also very amenable to prior information, such as theoretical predictions.

REFERENCES

1. Baum, C. E., "On the Singularity Expansion Method for the Solution of Electromagnetic Interaction Problems," Interaction Note 88, Air Force Weapons Laboratory, Kirtland AFB, NM, December 1971.

2. Lin, C. A., and J. T. Cordaro, "Singularity Expansion Method Parameter Measurement," Interaction Note 409, Air Force Weapons Laboratory, Kirtland AFB, NM, May 1981.

3. Pagano, M., "When is an Autoregressive Scheme Stationary?" Communications in Statistics, 1(6), 533-544, 1973.

4. Parzen, E., "Time Series Analysis for Models of Signal Plus White Noise," in Advanced Seminar on Spectral Analysis of Time Series, B. Harris, ed., John Wiley and Sons, New York, 1967.

5. Pagano, M., "Estimation of Models of Autoregressive Signal Plus White Noise," The Annals of Statistics, Vol. 2, 99-108, 1974.

6. Pond, J. M., and T.B.A. Senior, "Determinaton of SEM Poles from Frequency Responses," Interaction Note 408, Air Force Weapons Laboratory, Kirtland AFB, NM, July 1981.

7. Box, G.E.P., and G. M. Jenkins, Time Series Analysis: Forecasting and Control, Revised Edition, Holden Day Publishers, San Francisco, 1976.

8. Bingham, C., M. D. Godfrey, and J. W. Tukey, "Modern Techniques of Power Spectrum Estimation," IEEE Trans. Audio Electroacoustics, AU-15, 56-66, 1967.

9. Bloomfield, P., Fourier Analysis of Time Series: An Introduction, John Wiley and Sons, New York, 1976.